Assessing the role of the San Andreas fault in controlling the spatial distribution of erosion rates in the Transverse Ranges, southern California

Megan Mueller

Advised by Nathan Niemi

Department of Earth and Environmental Sciences, University of Michigan

April 2013

Abstract

In considering erosion rate controls, previous work has focused primarily on the geomorphic factors; here tectonic controls, particularly seismic shaking, are additionally considered, given the growing recognition that earthquakes may play a key role in generating landslides and erosion. We present new cosmogenic radionuclide data from the San Gabriel Mountains, combined with previously published data from the San Gabriel and San Bernardino Mountains, to resolve the parameters controlling erosion. Statistical analysis of erosion rate parameters reveals that one of the primary erosion rate controls in the San Gabriel and San Bernardino Mountains is catchment distance from the San Andreas fault, an analog for seismic shaking from the San Andreas fault. We hypothesize that seismically induced erosion plays a significant role in the sediment budget of the San Gabriel and San Bernardino Mountains.

Introduction

Erosion rate controls are studied to better understand the geomorphic, tectonic and atmospheric processes influencing orogenesis and landscape formation. Many techniques exist to calculate erosion rate, of which cosmogenic radionuclides (CRNs), low-temperature thermochronometry, and infilling of dams and debris basins are most common. CRN determine erosion rates over 10^2 – 10^6 yr timescales using in-situ cosmogenic ^{10}Be concentrations in fluvial and alluvial sediments (Niemi, unpub. data; Binnie et al., 2008, Niemi et al., 2005; Granger et al., 1996). Cosmogenic radionuclide dating is applicable in quantifying catchment erosion rates and in assessing the parameters controlling erosion. Low-temperature theromchronometric exhumation rates are calculated through apatite (U-Th)/He thermochronometry and apatite fission-track (AFT) on million-year timescales (Niemi et al., unpub. data). On decadal timescales, erosion rates are derived from infilling of dam and debris basins (Lavé and Burbank, 2004).

Processes influencing erosion rate include tectonic activity, catchment metrics, climate, bedrock erodibility, and stochastic mass-wasting (DiBiase et al., 2010; Niemi et al., unpub. data; Spotila et al., 2002). Studies suggest that erosion rate correlates with crustal displacement (Binnie et al., 2008; Binnie et al., 2010). Recent research has revealed the association between landslides and earthquakes, where landslide density and the distribution, duration and intensity of earthquake-induced ground shaking are linked (Ouimet, 2010; Meunier et al., 2013). Meunier et al. (2013) finds that, for two Japanese earthquakes, there is a link between the distributions of co-seismic landslides and fault slip. Additionally, Ouimet (2010) suggests that earthquakes are a parameter controlling erosion rates of uplifting mountain ranges. The role of seismic shaking in erosion rate in the San Gabriel Mountains (SGM) and San Bernardino Mountains (SBM) has not yet been studied. In light of the proposed effects of tectonic activity on erosion rate, this study deems catchment distance from the San Andreas fault a necessary parameter to consider in constraining erosion rate controls. We expect erosion rate to decrease as catchment distance from the SAF increases.

The influence of catchment metrics, like area, catchment-mean slope and channel steepness index, on erosion rate has been evaluated in previous erosion rate studies in the San Gabriel and San Bernardino Mountains. DiBiase et al. (2010) found no relationship between CRN-derived erosion rate and catchment area; however, Niemi et al. (2005) and Yanites et al. (2009) found that CRN-derived erosion rates are highly variable in small catchments and converge to a mean erosion rate at larger catchment scales. Catchment-mean slope and erosion rate have been well studied in the SGM and SBM (Spotila et al., 2002; Binnie et al., 2007; DiBiase et al., 2010). Slope is positively, linearly correlated with erosion rate until a threshold slope, after which slope and erosion rate decouple (Binnie et al., 2007; DiBiase et al., 2010). In the SGM, DiBiase et al. (2010) finds the threshold slope to be ~35°, corresponding to erosion rates above 300 m/My. Binnie et al. (2007) finds a threshold slope of ~30° in the SBM.

Uplift, bedrock erodibility, and precipitation are some controls on the topography of river channels. Channel steepness index is a metric used to quantify the effects of topography on river channels, and is hypothesized to reflect erosion rate (DiBiase et al., 2010). The channel steepness index is the ratio of uplift to erodibility (Perron and Royden, 2012). Wobus et al. (2006) investigated channel steepness in the San Gabriel Mountains, and, although unable to quantify the relationship between uplift and erodibility, they confirm that high uplift and exhumation rates trend with high channel steepness indices. Because of the gradient of increasing uplift from west to east in the SGM, channel steepness should increase from west to east, agreeing with DiBiase et al. (2010). In the SBM, channel steepness is not a reliable metric because erosion is controlled by stochastic mass-wasting events (DiBiase et al., 2010), particularly in high relief terrain near the San Andreas fault.

Precipitation is commonly considered when evaluating the role of climate in erosion rates, but its significance is debated. DiBiase et al. (2010) concludes that precipitation is spatially homogenous throughout the SGM, and therefore precipitation is not evaluated as an erosional control. Binnie et al. (2010) found no correlation between precipitation and erosion rate, but established that precipitation is needed in order to facilitate sediment transport. Finally, Spotila et al. (2002) found a strong correlation between precipitation and erosion rate in the two ranges, but acknowledged uncertainties in erosion rate as caused by the response of vegetation to precipitation, the difference between snow and rainfall, and orographically caused precipitation changes throughout the uplift history. The quantity of snowfall and the elevation of the mean annual snow line are important additional considerations, as snow lowers the production of CRNs in bedrock and leads to apparent higher erosion rates (Binnie et al., 2010; Schildgen et al., 2005).

Bedrock erodibility is hypothesized to play a role in erosion rate, where catchments of more easily erodible lithologies exhibit higher erosion rates, but this has not been well quantified (Spotila et al., 2002; Duvall et al., 2004). Finally, stochastic mass-wasting events, such as bedrock landslides, are known to influence erosion rates (Niemi et al., 2005; Niemi et al., unpub. data; Binnie et al., 2010). For small catchments, stochastic mass-wasting events greatly influence erosion rates resolved by CRN. Although Binnie et al. (2007) presents reliable CRN-derived erosion rates for catchments as small as 1-3 km^2, it is uncertain whether erosion rates derived from small catchments are indicative of long term averages.

This study employs CRNs from the SGM and SBM to evaluate catchment metrics and tectonic activity, attempting to establish the parameters primary controlling erosion rate. New CRN data from the SGM is complied with CRN data from DiBiase et al. (2010) and Binnie et al. (2008), representing one of the largest CRN erosion rate datasets.

Geological Setting

The San Gabriel and San Bernardino Mountains of the central Transverse Ranges in southern California straddle Big Bend, a restraining bend of the dextral San Andreas fault (SAF). The development of these ranges is linked to the evolution of the Big Bend of the SAF, the abandonment of the San Gabriel fault as the active plate boundary fault, and the establishment of the modern SAF (Powell and Weldon, 1992). Present-day exhumation of the SGM and SBM is a result of compression along Big Bend (e.g. Blythe et al., 2002; Blythe et al., 2000).

The SBM are bounded by the SAF to the north and the Cucamonga and Sierra Madre thrusts to the south. In the western SGM, over 50% of the north-south shortening is accommodated by strike-slip faults, not the thrust systems along the SAF (Walls et al., 1998). The SGM exhibit a strong west to east gradient of increasing uplift and exhumation (Blythe et al., 2002). The San Bernardino Mountains are bound by the SAF to the south and the Northern Frontal System to the north (Binnie et al., 2010).

The SGM are primarily Proterozoic metamorphic and igneous rocks, and the SBM are Cretaceous plutonic rocks. Previous studies have used the uniformity in lithology and precipitation to isolate relief and erosion (e.g. DiBiase et al., 2010). To a first-order approximation, lithology, and therefore bedrock erodibility, can be considered homogenous within the SGM and within the SBM. However, snow shielding and precipitation are proposed to influence erosion rate, but have not been quantified (Binnie et al., 2010; Spotila et al., 2002). Precipitation in the two ranges increases by a factor of about 2 from the southern range front to the range crest (Spatial Climate Analysis Services; Minnich, 1986).

Methods

Cosmogenic Sample Collection, Preparation, and Analysis

Nathan Niemi collected stream sediment from active channel beds in the San Gabriel Mountains. Samples underwent wet-sieve and heavy liquid separation, and then were etched to yield pure quartz separates. The separates were then processed to remove fluorides, iron, titanium, and other contaminants. The $^{10}Be/^{9}Be$ ratio was measured by the Scottish Universities Environmental Research Centre's accelerator mass spectrometer; measurements were normalized to a NIST SRM 4325 standard with an assumed $^{10}Be/^{9}Be$ ratio of 3.06×10^{-11}.

Erosion Rate Synchronization

This study presents new cosmogenic radionuclide data for the San Gabriel Mountains in combination with SGM CRN data from DiBiase et al. (2010) and SBM CRN data from Binnie et al. (2008). To compare the erosion rate among the three datasets, erosion rates were recalculated from published ^{10}Be concentrations and lab specific chemistry standards using the University of Washington's online CRONUS-Earth surface erosion rate calculator version 2.2 (http://hess.ess.washington.edu) (Table 1).

Parameter Estimation

In ArcGIS version 10, catchment and stream profile data was extracted from a 3 meter resolution TOPSAR digital elevation model (DEM) of the San Gabriel Mountains and a 10 meter resolution USGS NED DEM of the San Bernardino Mountains. Catchments for each of the CRN sample locations were delineated by first creating a hillshade raster, hydrologically correcting the DEM to remove any aberrant sinks or highs, and creating a flow accumulation raster. Noise in the high resolution SBM DEM may have led to artifacts in the DEM, and therefore minor inaccuracies in catchment delineation. Then the flow accumulation raster was used to define the streams, which we chose to define as having a flow accumulation of greater than 2500 m^2. A flow direction raster was created and used to define the catchments. Finally, for each catchment, the stream raster was clipped to only include the largest stream in each catchment and the upstream length for each of the largest streams was extracted. For each catchment, area, slope, centroid, and elevation statistics were extracted (Table 2). Figure 1 displays each catchment colored by erosion rate.

From the DEMs, we approximated the trace of the SAF through the SGM and SBM, from which the perpendicular distance from the catchment centroid to the SAF and the catchment centroid's parallel distance along the SAF were calculated. These two distance measurements are used as a proxy for seismic shaking along the SAF in erosion rate.

Table 1: Cosmogenic Radionuclide Data for the San Gabriel and San Bernardino Mountains.

Sample*	Easting†	Northing†	^{10}Be Concentration (atoms/g)	Error (atoms/g)	Published Erosion Rate (m/My)	Error (m/My)	Recalibrated Erosion Rate (m/My)	Error (m/My)
1001	438022.3	3781734.0	1.870E+05	5.700E+04	670	190	62.51	21.53
1003	437817.2	3785550.0	2.220E+05	1.600E+04	620	70	58.46	5.97
1005	439813.9	3788614.1	1.830E+05	1.800E+04	830	110	78.10	9.62
1007	441539.1	3789692.1	1.210E+05	1.500E+04	1260	190	117.39	17.38
1009	441637.4	3789941.0	2.030E+05	2.100E+04	840	110	79.86	10.11
1011	439269.7	3788332.7	4.020E+05	4.700E+04	300	40	30.08	4.07
1012	395795.2	3797831.6	2.630E+05	4.500E+04	310	50	33.38	6.39
1013	437748.7	3785768.9	9.700E+04	1.400E+04	880	130	85.25	14.52
1014	437655.8	3784687.2	2.740E+05	1.800E+04	280	30	31.64	3.08
1015	437623.5	3784127.4	1.950E+05	1.900E+04	430	50	43.31	5.33
1016	437659.1	3782961.8	2.230E+05	1.200E+04	360	40	36.53	3.28
1017	437432.8	3780256.5	2.100E+05	2.100E+04	350	40	53.39	6.63
1018	395530.3	3797593.9	2.510E+05	2.300E+04	340	40	35.43	4.16
1019	397125.6	3798980.3	6.310E+05	6.100E+04	150	20	14.45	1.74
1020	398018.3	3800857.0	7.300E+05	4.700E+04	130	10	12.57	1.22
1021	398706.7	3803424.7	6.890E+05	4.600E+04	140	20	13.99	1.37
1022	398956.8	3805293.0	5.680E+05	9.200E+04	180	30	18.37	3.27
2001	393590.0	3796490.0	7.321E+04	1.460E+04	109	27	124.83	28.89
2002	398070.0	3796470.0	6.903E+04	1.725E+04	119	36	135.57	39.53
2003	396850.0	3797050.0	9.674E+04	1.399E+04	84	16	96.89	16.53
2004	405576.0	3793270.0	2.443E+05	2.434E+05	35	37	41.32	10.53
2005	396964.0	3799133.0	5.653E+04	1.086E+04	135	33	156.05	35.17
2006	385052.0	3799080.0	2.939E+04	1.246E+04	246	117	283.22	161.31
2007	394360.0	3795594.0	2.916E+04	4.740E+03	253	54	289.96	57.06
2008	384501.0	3796261.0	1.533E+04	5.600E+02	424	37	497.10	41.39
2009	389930.0	3793860.0	2.256E+04	7.600E+02	279	23	330.72	27.04
2010	431950.0	3795090.0	1.482E+04	6.700E+02	826	79	860.39	76.60
2011	429900.0	3789052.0	1.107E+04	6.300E+02	1010	108	1063.41	100.87
2012	431750.0	3795109.0	2.822E+04	1.840E+03	436	50	442.43	46.17
2013	406050.0	3793401.0	2.715E+04	2.540E+03	314	45	350.43	44.63
2014	405531.0	3793280.0	3.318E+04	3.350E+03	265	32	288.98	37.02
2015	403550.0	3801480.0	9.368E+04	3.950E+03	108	32	119.84	10.32
2016	403580.0	3800022.0	5.255E+04	3.060E+03	151	16	174.53	16.86
2017	400471.0	3785950.0	1.614E+04	1.320E+03	465	61	530.35	61.82
2018	400230.0	3786700.0	1.294E+04	9.000E+02	591	71	678.48	71.67
2019	400100.0	3786719.0	1.026E+04	8.700E+02	736	99	856.79	100.31
2020	407130.0	3799908.0	2.507E+05	2.068E+04	42	6	47.69	5.22
2021	406977.0	3800170.0	2.138E+05	5.730E+04	49	16	55.69	16.57
2022	408940.0	3804594.0	1.385E+05	9.040E+03	73	8	82.21	8.16
2023	408762.0	3802978.0	1.029E+05	1.270E+04	98	17	109.42	16.33
2024	409009.0	3802950.0	9.448E+04	4.540E+03	106	10	118.55	10.59
2025	427489.0	3798670.0	1.031E+05	4.450E+03	144	13	151.40	13.29
2026	418150.0	3792511.0	1.505E+04	1.400E+03	591	84	643.89	81.05
2027	417980.0	3792440.0	1.865E+04	2.750E+03	428	85	474.82	85.89
2028	412561.0	3790543.0	3.249E+04	1.990E+03	189	21	235.29	23.28

Table 1: Cosmogenic Radionuclide Data for the San Gabriel and San Bernardino Mountains.

Sample*	Easting†	Northing†	^{10}Be Concentration (atoms/g)	Error (atoms/g)	Published Erosion Rate (m/My)	Error (m/My)	Recalibrated Erosion Rate (m/My)	Error (m/My)
2029	410390.0	3790543.0	3.045E+04	2.380E+03	292	37	316.03	35.96
2030	405510.0	3793789.0	2.382E+04	2.570E+03	323	51	388.60	54.72
2031	426461.0	3793780.0	3.482E+04	1.027E+04	434	150	432.16	151.75
2032	426300.0	3798089.0	1.993E+05	9.520E+03	79	8	83.76	7.36
2033	432789.0	3796090.0	1.168E+04	1.570E+03	1106	204	1155.73	183.91
2034	432614.0	3796111.0	1.168E+04	1.390E+03	1039	175	1107.13	160.74
2035	431831.0	3795020.0	1.715E+04	1.670E+03	717	106	739.45	95.21
2036	429939.0	3795791.0	1.203E+04	1.690E+03	1006	191	1074.76	178.44
2037	441441.0	3780431.0	3.369E+04	4.630E+03	279	52	293.55	49.71
2038	441440.0	3780432.0	4.313E+04	2.830E+03	218	25	230.64	23.77
2039	408889.0	3802380.0	1.600E+04	2.180E+03	617	115	673.05	112.29
2040	408780.0	3802535.0	8.934E+04	5.770E+03	110	13	122.22	12.24
2041	427120.0	3787967.0	1.856E+04	5.210E+03	277	91	346.77	119.90
2042	425810.0	3788950.0	2.304E+04	2.330E+03	265	40	313.29	41.97
2043	408768.0	3802844.0	8.127E+04	3.490E+03	119	11	132.76	11.51
2044	405524.0	3804763.0	1.676E+05	8.310E+03	78	8	84.89	7.57
2045	398617.0	3796775.0	1.254E+04	8.300E+02	605	70	693.42	71.32
2046	417222.0	3802455.0	1.109E+05	6.080E+03	118	12	126.55	11.87
2047	416848.0	3802226.0	1.551E+05	7.650E+03	87	9	93.85	8.39
2049	411172.0	3798020.0	7.864E+04	4.280E+03	147	15	158.59	14.96
2050	409731.0	3796134.0	4.270E+04	2.890E+03	239	28	256.20	26.94
3001	502906.1	3771525.7	5.600E+03	1.100E+03	2200	500	2241.42	492.56
3002	505369.2	3771792.9	4.70E+03	8.60E+03	2700	500	2969.58	578.44
3004	505602.0	3768056.4	1.01E+04	1.10E+03	1200	200	1212.72	165.52
3005	504114.4	3772069.4	1.10E+04	1.20E+03	1100	200	1064.18	145.04
3006	501549.7	3772634.2	4.20E+04	3.90E+03	270	28	219.87	26.80
3008	503410.5	3779886.2	2.21E+04	1.50E+03	560	60	522.87	54.92
3009	501778.4	3782713.2	1.03E+04	1.30E+03	1200	200	1165.07	176.29
3010	502147.0	3782691.1	2.08E+04	1.90E+03	660	80	611.00	75.02
3011	504764.1	3782392.7	2.68E+04	2.00E+03	520	60	483.21	53.53
3012	498866.9	3785252.3	7.44E+04	5.20E+03	170	20	163.31	17.64
3013	494774.3	3781029.1	7.70E+03	1.30E+03	1600	300	1496.21	286.12
3014	506283.9	3783513.5	6.20E+04	3.00E+03	230	20	214.50	20.54
3016	494999.6	3805844.7	1.01E+05	6.10E+03	100	10	99.51	10.04
3017	493041.9	3806145.3	1.11E+05	7.20E+03	89	10	86.89	9.01
3018	497137.3	3792715.1	9.73E+04	5.50E+03	150	20	145.08	14.69
3019	494192.0	3793060.2	1.28E+05	5.80E+03	97	9	94.45	8.93
3020	496189.4	3793203.3	1.81E+05	1.00E+04	71	7	70.21	7.09
3021	494246.5	3806953.9	8.42E+04	6.50E+03	129	15	124.21	13.92
3022	491596.7	3803718.1	2.15E+05	9.40E+03	52	5	52.28	4.95

*Sample numbers 1000 are the new data from the SGM, samples 2000 are in the SGM from DiBiase et al. (2010), and samples 3000 are in the SBM from Binnie et al. (2008).

†UTM NAD 27.

Table 2: Catchment Locations and Metrics.

Catchment	Centroid Easting	Centroid Northing	Area (km^2)	Mean Slope (°)	Minimum Elevation (m)	Maximum Elevation (m)	Range Elevation (m)	Mean Elevation (m)	Steepness Index m/n 0.38	Steepness Index m/n 0.47	Perpendicular Distance (m)	Parallel Distance (m)
1001	440476.219	3788701.037	57.40	32.68	745.03	3070.31	2325.28	1836.65	0.3227	0.3992	12016.20	7298.81
1003	441090.500	3790129.184	46.10	32.49	976.14	3070.31	2094.17	1995.12	0.3388	0.3961	10464.75	7399.43
1005	442321.520	3790612.251	30.36	32.67	1320.81	3070.31	1749.51	2164.14	0.3552	0.3854	9476.22	6521.62
1007	443515.786	3789685.921	10.95	32.38	1522.13	2733.40	1211.27	2181.21	0.2136	0.2195	9760.69	5037.06
1009	440614.429	3793046.925	11.14	32.89	1540.08	3070.31	1530.23	2364.22	0.3441	0.3529	8079.64	9147.59
1011	439029.444	3790158.761	4.68	32.41	1282.78	2555.89	1273.11	1860.42	0.2438	0.2474	11372.49	9249.52
1012	394154.712	3801721.641	14.94	29.23	941.37	1983.11	1041.74	1375.87	0.1282	0.1390	21403.32	54485.35
1013	437472.339	3786176.974	0.22	37.92	1064.39	1698.37	633.98	1308.69	0.1781	0.1509	15627.56	8830.36
1014	436501.112	3784968.491	1.37	36.21	956.33	1705.51	749.18	1360.98	0.1607	0.1553	17144.98	9147.50
1015	436664.161	3784160.885	1.01	35.44	906.70	1679.39	772.69	1323.74	0.2655	0.2497	17790.98	8635.76
1016	436096.873	3783310.475	1.24	36.24	853.15	1677.28	824.13	1267.27	0.0286	0.0263	18806.14	8755.41
1017	440475.500	3789705.121	63.96	32.48	681.17	3070.31	2389.15	1764.20	0.3166	0.3966	11121.49	7755.06
1018	397060.115	3801856.180	56.21	27.55	925.75	2018.80	1093.05	1395.61	0.0994	0.1161	19966.61	51957.31
1019	399184.009	3803289.701	28.49	26.59	1018.41	2018.80	1000.38	1449.04	0.0993	0.1120	17726.19	50715.11
1020	399373.936	3804776.011	18.08	25.95	1101.33	2018.80	917.47	1465.46	0.1007	0.1086	16315.21	51220.27
1021	399477.604	3804870.105	11.96	25.78	1204.07	2018.80	814.73	1531.20	0.1021	0.1026	16184.35	51170.58
1022	398629.506	3806123.642	1.71	25.83	1353.72	1762.74	409.01	1576.37	0.1217	0.1123	15451.32	52495.14
2001	401000.938	3799356.643	170.45	25.44	742.32	2172.59	1430.28	1412.06	0.1541	0.2024	20408.66	47311.37
2002	403361.416	3798130.780	101.92	23.80	978.58	2172.59	1194.01	1453.73	0.1192	0.1487	20431.58	44651.64
2003	399462.233	3796413.735	107.00	23.94	926.06	2172.59	1246.53	1443.11	0.1279	0.1623	23729.33	47347.21
2004	407122.581	3794187.322	5.62	23.03	1300.99	1795.32	494.33	1528.93	0.0877	0.0887	22242.16	39510.61
2005	396067.303	3802723.243	9.94	28.00	1020.48	1836.20	815.72	1363.16	0.1102	0.1210	19643.67	53235.46
2006	385805.686	3800424.877	9.68	32.04	848.53	1717.29	868.76	1290.81	0.1424	0.1360	26343.18	61337.01
2007	394881.616	3794865.653	3.16	33.62	935.21	1695.52	760.31	1318.84	0.1513	0.1451	27185.31	50726.69
2008	385392.091	3799541.120	17.33	32.74	524.67	1717.29	1192.62	1143.47	0.1685	0.1792	27318.41	61304.57
2009	391080.599	3793292.130	7.48	31.65	652.71	1692.67	1039.96	1113.53	0.1113	0.1134	30310.63	53399.90
2010	435633.840	3798938.054	82.67	33.61	938.43	3070.58	2132.16	1957.94	0.0669	0.0836	5085.57	16259.04
2011	432654.630	3797535.154	148.63	34.34	605.45	3070.58	2465.14	1807.75	0.1446	0.1629	7686.34	18277.34
2012	428370.815	3798415.724	35.00	34.92	939.36	2864.65	1925.30	1963.04	0.2666	0.3146	8842.90	22494.33
2013	406142.961	3794405.839	1.10	22.64	1330.15	1731.29	401.14	1517.56	0.1039	0.0956	22491.35	40482.73
2014	407075.897	3794156.764	5.94	23.17	1299.98	1795.32	495.35	1525.94	0.0885	0.0897	22290.56	39538.35
2015	404910.755	3803904.928	3.18	27.67	1340.22	2172.59	832.38	1736.87	0.1554	0.1592	14582.32	45891.00
2016	402547.985	3800641.523	0.31	25.45	1263.54	1695.90	432.36	1431.23	0.0399	0.0342	18562.16	46515.76
2017	401268.204	3786615.018	1.96	34.23	899.80	1764.28	864.48	1339.48	0.2413	0.2364	31645.41	41291.69
2018	400859.889	3787752.527	2.28	36.43	964.74	1749.21	784.48	1367.73	0.1786	0.1728	30816.49	42171.69
2019	399479.720	3788250.040	2.59	37.00	940.09	1876.47	936.39	1351.68	0.1778	0.1746	30998.53	43627.35
2020	406615.027	3801075.210	2.17	16.20	1709.95	1897.50	187.55	1790.50	0.0231	0.0224	16332.32	43088.29
2021	406626.818	3800505.679	0.13	17.24	1720.02	1870.86	150.84	1791.36	0.0632	0.0516	16834.66	42819.35
2022	408664.635	3805304.094	0.29	24.31	1632.32	1863.48	231.16	1739.87	0.0449	0.0389	11633.78	43180.67
2023	408310.292	3802066.731	2.31	17.99	1610.75	1870.61	259.86	1737.41	0.0485	0.0470	14680.16	42027.49
2024	409246.004	3802262.623	1.15	19.05	1600.81	1878.50	277.69	1733.09	0.0616	0.0574	14081.46	41282.53
2025	427149.698	3798909.889	0.12	27.34	2176.78	2379.44	202.66	2279.38	0.0992	0.0806	8955.83	23806.73
2026	418804.859	3798065.553	46.77	34.05	665.15	2516.81	1851.66	1531.33	0.2089	0.2457	13490.50	30859.94
2027	415215.439	3795077.778	17.91	35.10	667.55	2371.99	1704.43	1397.04	0.1972	0.2195	17780.59	32702.87
2028	412787.200	3792254.119	6.02	31.64	719.78	1677.42	957.64	1146.41	0.1840	0.1868	21398.11	33585.52
2029	410893.911	3795556.009	42.87	30.67	743.73	2450.18	1706.45	1534.02	0.1808	0.2135	19312.88	36770.91

Table 2: Catchment Locations and Metrics.

Catchment	Centroid Easting	Centroid Northing	Area (km^2)	Mean Slope (°)	Minimum Elevation (m)	Maximum Elevation (m)	Range Elevation (m)	Mean Elevation (m)	Steepness Index m/n 0.38	Steepness Index m/n 0.47	Perpendicular Distance (m)	Parallel Distance (m)
2030	405654.531	3794165.567	0.15	20.95	1355.10	1658.67	303.57	1473.11	0.0627	0.0513	22926.90	40808.96
2031	426034.584	3798874.746	4.03	31.08	1822.54	2697.74	875.21	2269.26	0.1826	0.1826	9492.55	24784.49
2032	425816.597	3799357.291	2.10	31.07	1982.25	2697.74	715.49	2345.55	0.1820	0.1764	9161.20	25197.70
2033	439276.566	3795902.863	25.44	34.68	1028.87	3070.58	2041.71	2022.70	0.3381	0.3821	6140.19	11635.68
2034	432619.268	3800546.920	53.34	32.70	1025.50	2942.55	1917.05	1955.27	0.0090	0.0232	5017.68	19675.44
2035	428372.767	3798413.887	35.02	34.92	933.42	2864.65	1931.23	1962.45	0.2667	0.3152	8843.65	22491.75
2036	426966.833	3797401.716	11.55	35.62	1160.09	2697.74	1537.65	1959.04	0.2501	0.2751	10383.09	23285.35
2037	442748.803	3784753.175	27.94	34.39	658.57	2695.06	2036.49	1580.28	0.2906	0.3406	14505.35	3482.31
2038	442748.803	3784753.175	27.94	34.39	658.57	2695.06	2036.49	1580.28	0.2906	0.3406	14505.35	3482.31
2040	408885.784	3802406.672	0.13	14.67	1649.09	1738.62	89.53	1694.16	0.0276	0.0228	14116.31	41668.90
2041	427170.217	3786747.985	5.40	31.32	512.53	1143.72	631.20	864.28	0.1036	0.1088	19787.66	18269.98
2042	427160.505	3790861.096	6.53	34.46	529.85	1772.74	1242.89	1057.53	0.2260	0.2422	16125.63	20144.96
2043	408782.548	3802544.605	0.19	14.94	1622.60	1738.62	116.02	1679.21	0.0379	0.0318	14040.15	41823.48
2044	405175.940	3805046.368	0.18	21.71	1991.96	2174.45	182.48	2091.53	0.0867	0.0716	13444.65	46172.61
2045	398966.358	3794431.942	9.59	29.11	1000.96	1874.26	873.30	1348.10	0.1195	0.1279	25720.64	46889.86
2046	415396.830	3801351.971	9.03	25.53	1725.38	2450.96	725.58	2096.11	0.1409	0.1431	12105.56	35388.14
2047	415396.830	3800811.703	5.29	24.67	1762.24	2450.96	688.72	2135.37	0.1387	0.1394	12587.15	35143.00
2049	411519.500	3799777.604	2.08	25.60	1401.51	2303.57	902.06	1921.12	0.2351	0.2308	15266.22	38128.98
2050	412778.026	3798754.203	21.77	28.37	1160.06	2450.18	1290.12	1735.33	0.1779	0.1947	15608.10	36543.10
3001	503589.798	3771025.328	1.38	30.51	1531.17	2385.82	854.66	1924.71	0.0926	0.0713	831.81	56963.89
3002	505532.781	3770995.102	1.02	34.29	1584.26	2485.66	901.40	2078.30	0.1510	0.1180	1685.46	58709.05
3004	505765.933	3768501.358	1.08	37.33	1554.41	2455.02	900.61	1940.41	0.1149	0.0888	431.80	60048.36
3005	504181.935	3771602.774	0.60	37.38	1509.78	2300.64	790.85	1878.25	0.1428	0.1045	1614.91	57229.54
3006	501912.861	3771790.115	0.79	25.78	1223.84	1820.23	596.39	1529.13	0.0914	0.0703	753.52	55122.50
3008	503963.326	3779331.388	0.41	25.15	1603.93	2140.35	536.42	1908.87	0.0882	0.0648	8405.12	53527.88
3009	501633.988	3783863.940	2.75	32.08	1497.69	2417.44	919.75	1905.00	0.0865	0.0706	11389.75	49395.49
3010	503015.884	3784006.551	3.60	27.96	1527.53	2441.29	913.76	2056.05	0.1421	0.1169	12143.17	50562.23
3011	504386.517	3783977.853	2.93	26.43	1587.78	2441.21	853.42	2097.32	0.1203	0.1002	12738.78	51796.66
3012	497702.745	3785988.305	3.09	30.94	1442.04	2392.37	950.33	1954.49	0.0761	0.0641	11501.70	44928.32
3013	496414.935	3782947.749	4.16	32.14	1109.83	2407.28	1297.45	1814.74	0.1300	0.1120	8207.69	45160.36
3014	505637.869	3784609.866	1.53	26.91	1714.15	2416.11	701.96	2117.62	0.0899	0.0715	13869.29	52625.00
3016	495123.345	3805019.598	1.29	24.53	1349.16	1799.26	450.10	1620.11	0.0613	0.0473	27297.17	33994.30
3017	492900.271	3805336.689	1.75	21.71	1310.15	1679.55	369.40	1548.86	0.0439	0.0343	26572.29	31869.37
3018	497402.897	3791279.832	2.50	23.19	1817.83	2548.76	730.93	2186.72	0.0807	0.0666	16082.67	42260.09
3019	496476.898	3795055.001	8.06	16.16	1622.16	2209.82	587.66	1912.33	0.0383	0.0333	19028.18	39721.92
3020	497304.558	3793954.672	8.81	10.94	1721.83	2346.02	624.19	1973.75	0.0299	0.0253	18422.46	40958.75
3021	495258.167	3803606.681	6.33	19.37	1174.56	2162.67	988.11	1694.06	0.0706	0.0600	26098.80	34755.55
3022	492941.295	3802365.002	7.64	10.58	1507.02	2161.71	654.68	1765.89	0.0257	0.0206	23941.92	33254.33

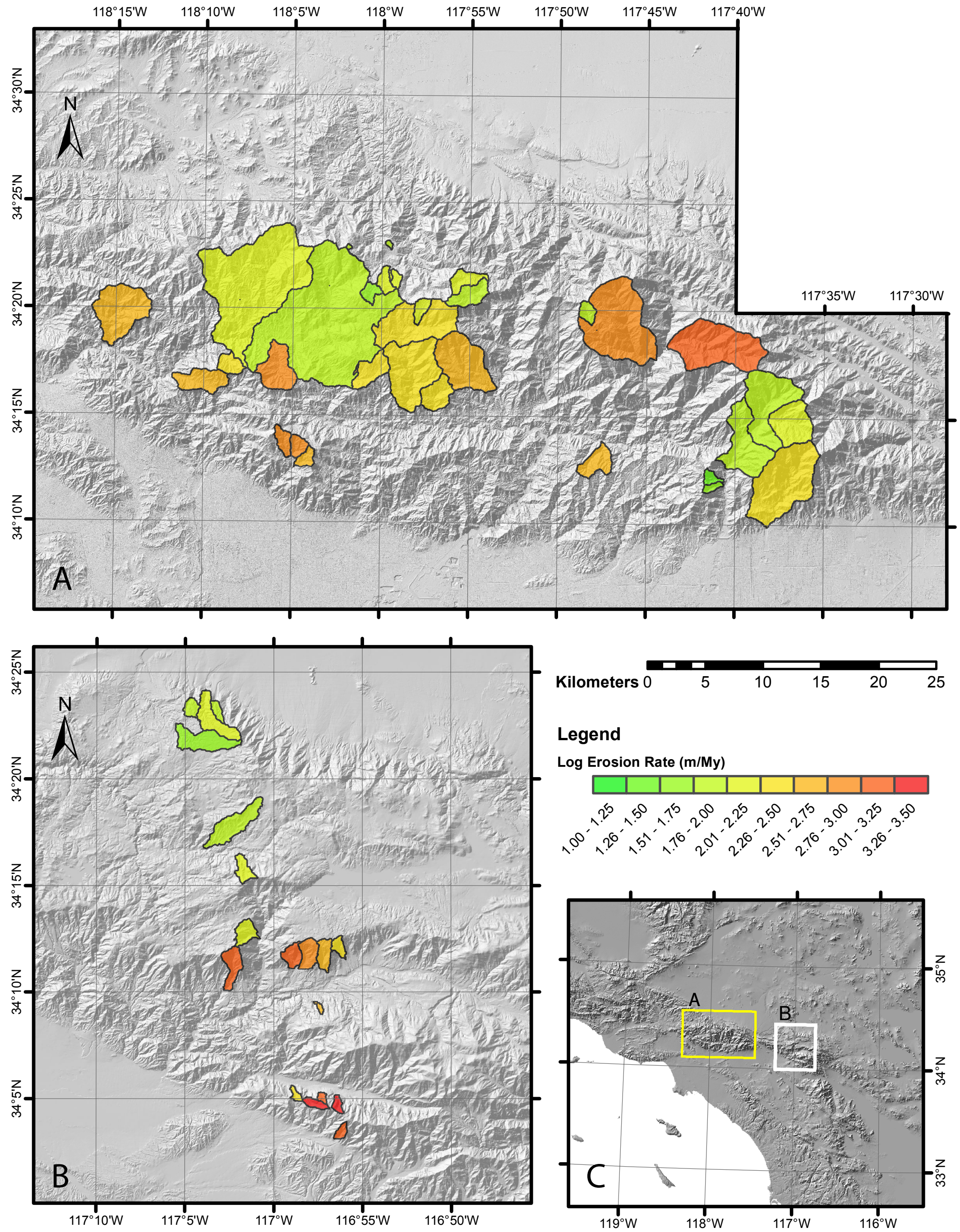

Figure 1: A. Hillshade DEM of the San Gabriel Mountains with catchments colored by the log of erosion rate. B. Hillshade DEM of the San Bernardino Mountains with catchments colored by the log of erosion rate. Note the north to south increase in erosion rate. C. Inset map from the USGS.

Channel Steepness Index

The stream power model evaluates bedrock river erosion rate as a function of channel slope and drainage area:

$$\frac{\partial \mathrm{z}}{\partial \mathrm{t}} = \mathrm{U(x,t)} - \mathrm{K(x,t)A(x,t)^m} \left|\frac{\partial \mathrm{z}}{\partial \mathrm{t}}\right|^{\mathrm{n}}$$

where *z* is elevation, *x* is upstream distance, *t* is time, *U* is uplift rate, *K* is erodibility, *A* is drainage area, and *m* and *n* are constants. To linearize stream profiles, Perron and Royden (2012) transformed the stream power equation assuming steady-state topography, uniform uplift, and uniform erodibility:

$$z(x) = z(x_b) + \left(\frac{U}{K}\right)^{\frac{1}{x}} \chi$$

where $\chi = \int_{x_b}^{x} \left(\frac{A}{A(x)}\right)^{\frac{m}{n}} dx$, A_0 is a reference drainage area, and x_b is a base level point. The stream profile transformation reduces the noise seen in typical slope-area analyses, and evaluates river profiles independent of catchment area. Perron and Royden (2012) demonstrate the feasibility of using this method to analyze steady-state and transient profiles, and the effects of lithology, climate and tectonics on stream profiles.

The stream power equation linearization is employed to calculate the channel steepness index for each catchment in the SGM and SBM. For each stream profile extracted from this study's catchments, χ was calculated at range of m/n values from zero to one, and then a least-squares regression of elevation was performed for each χ value. Finally, the m/n value with the highest R^2 is recorded as the best m/n value, and χ for the best m/n value is determined. The average best m/n value is 0.38, and 0.47 for all non-zero best m/n values. The plot of elevation against χ is known as a chi plot, where the slope of a chi plot is the steepness index. The steepness index, the ratio of uplift, *U*, to erodibility, *K*, at the two average m/n values, 0.38 and 0.47, is extracted for each river profile. Figure 2 displays each catchment

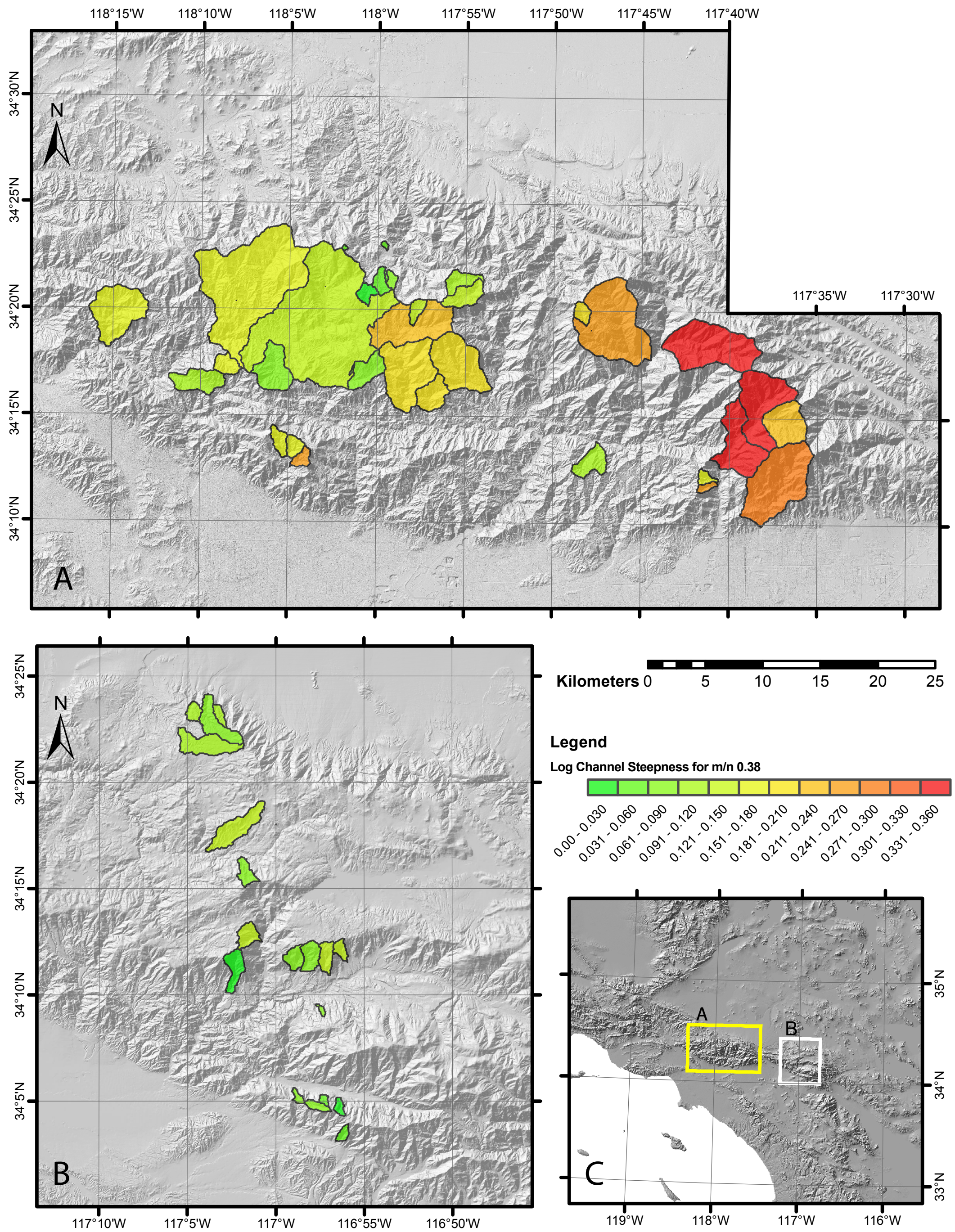

Figure 2: A. Hillshade DEM of the San Gabriel Mountains with catchments colored by the log of channel steepness index for m/n 0.38. Note the west to east increase in channel steepness rate.
B. Hillshade DEM of the San Bernardino Mountains with catchments colored by the log of channel steepness index for m/n 0.38. Any trends, or lack thereof, are the same for m/n 0.38 and 0.47. Note the lack of a spatial t end in channel steepness. C. Inset map from the USGS.

colored by the channel steepness index for m/n 0.38; any spatial trends, or lack thereof, are the same for m/n 0.38 and 0.47. High channel steepness indices correspond to high uplift and exhumation rates (Perron and Royden, 2012; Wobus et al., 2006). For each stream, the stream profile, the best fit m/n plot, and a chi plot is generated (Figure 3, Appendix A).

Statistics Methods

All statistical analyses are performed using the statistical software R. The statistical methods used for this study are similar to those employed by Lechler and Niemi (2012) in studying the environmental controls on isotopes in precipitation. In considering the factors controlling erosion rates in the SGM and SBM, linear fit models were created using these catchment variables: area, minimum elevation, maximum elevation, range in elevation, mean elevation, mean slope, mean slope squared, centroid latitude, centroid longitude, steepness indices for m/n 0.38 and 0.47, parallel distance from the SAF, and four functions of perpendicular distance from the SAF. In considering the perpendicular distance from the SAF, we considered the following four functions: the perpendicular distance, the inverse of perpendicular distance, the log of the inverse of perpendicular distance, and the square root of the inverse of perpendicular distance.

Erosion rate is modeled as a linear function of the above variables and the significance of each variable is evaluated; statistically significant variables have a p-value less than 0.05. Dropping the statistically insignificant variables from the full model creates subsequent linear fit models. These subsequent linear fit models, referred to as reduced models, are used to evaluate which parameters are most influential in controlling erosion rate. An analysis of variance evaluates whether the reduced model successfully replaces the full model. The full and reduced models are evaluated based on their goodness of fit of the model's predicted erosion rate with the actual erosion rate (Table 3). There are 8 full models, varying between the two m/n values and the four perpendicular distance functions. The

Table 3: Actual and Model Predicted Erosion Rates.

Catchment	Actual Erosion Rate (m/My)	Full Model 1 Predicted Erosion Rate (m/My)	Full Model 2 Predicted Erosion Rate (m/My)	Reduced Model 1 Predicted Erosion Rate (m/My)	Reduced Model 2 Predicted Erosion Rate (m/My)
1001	62.51	2957.91	1176.74	242.67	187.30
1003	58.46	3252.86	1477.38	275.91	217.80
1005	78.1	3613.83	1841.35	302.59	244.16
1007	117.39	3811.47	1999.00	268.16	192.87
1009	79.86	3871.95	2044.05	383.01	339.01
1011	30.08	3363.12	1594.24	267.08	215.31
1012	33.38	3174.19	1394.77	414.82	433.98
1013	85.25	3095.88	1418.70	403.68	562.31
1014	31.64	3072.38	1356.20	304.21	362.21
1015	43.31	2832.95	1114.70	255.68	268.55
1016	36.53	3176.86	1461.38	275.40	313.91
1017	53.39	2926.88	1194.78	261.59	204.55
1018	35.43	3073.16	1295.70	352.92	351.28
1019	14.45	3057.99	1268.92	343.54	352.36
1020	12.57	3173.34	1422.06	352.12	373.98
1021	13.99	3297.33	1538.93	348.69	370.61
1022	18.37	3310.10	1536.74	376.58	412.81
2001	124.83	2795.06	1032.35	233.80	183.71
2002	135.57	2946.21	1154.08	158.90	93.05
2003	96.89	2989.87	1172.75	146.63	47.52
2004	41.32	3275.94	1444.14	62.29	-53.62
2005	156.05	3180.45	1433.32	384.86	400.26
2006	283.22	3348.45	1563.20	525.79	576.20
2007	289.96	3352.73	1546.59	474.10	505.96
2008	497.1	3060.98	1286.68	542.11	598.35
2009	330.72	3128.44	1333.87	392.46	319.39
2010	860.39	3812.73	2139.42	614.58	584.30
2011	1063.41	3403.45	1724.67	545.38	600.91
2012	442.43	3632.03	1915.59	571.20	682.37
2013	350.43	3289.28	1464.49	57.99	-53.67
2014	288.98	3354.09	1545.16	65.90	-51.36
2015	119.84	3585.40	1831.97	387.18	411.68
2016	174.53	3251.66	1477.15	253.50	222.61
2017	530.35	3197.92	1325.23	362.28	287.27
2018	678.48	3546.73	1714.65	471.63	513.20
2019	856.79	3597.64	1779.21	509.44	583.99
2020	47.69	3730.54	1917.47	25.81	137.42
2021	55.69	3767.31	1971.53	35.44	107.60
2022	82.21	3585.32	1832.49	320.61	325.85
2023	109.42	3612.41	1837.17	82.60	149.65
2024	118.55	3499.48	1710.35	110.73	152.62
2025	151.4	4200.53	2380.30	298.23	212.96
2026	643.89	3137.43	1438.00	496.39	611.15
2027	474.82	3025.09	1274.59	478.87	608.05
2028	235.29	2674.29	927.95	296.60	260.17
2029	316.03	3142.94	1359.48	321.27	303.80
2030	388.6	3250.56	1415.64	11.68	-86.35
2031	432.16	4191.45	2392.98	421.77	415.40
2032	83.76	4260.39	2436.75	435.74	430.31
2033	1155.73	3391.12	1658.66	558.31	569.47
2034	1107.13	3852.96	2153.90	615.98	570.30
2035	739.45	3588.78	1861.02	571.01	682.01
2036	1074.76	3718.95	1970.36	562.29	711.88
2037	293.55	2880.97	1144.84	219.55	191.66
2038	230.64	2880.97	1144.84	219.55	191.66
2040	122.22	3638.57	1885.82	25.43	204.17
2041	346.77	2356.82	701.87	155.86	48.66
2042	313.29	2432.82	772.42	356.57	408.27
2043	132.76	3581.21	1827.17	33.40	202.72
2044	84.89	3972.72	2110.78	236.97	265.74
2045	693.42	3133.73	1303.39	283.12	192.88
2046	126.55	3859.18	2027.94	268.79	232.23
2047	93.85	3889.17	2036.21	229.22	187.10
2049	158.59	3589.16	1773.11	231.38	189.83
2050	256.2	3374.42	1585.67	298.85	273.77
3001	2241.42	4547.60	3082.47	1416.59	1110.48
3002	2969.58	4742.71	3221.77	1377.48	1380.87

Table 3: Actual and Model Predicted Erosion Rates.

Catchment	Actual Erosion Rate (m/My)	Full Model 1 Predicted Erosion Rate (m/My)	Full Model 2 Predicted Erosion Rate (m/My)	Reduced Model 1 Predicted Erosion Rate (m/My)	Reduced Model 2 Predicted Erosion Rate (m/My)
3004	1212.72	4853.43	3413.32	1911.79	1705.96
3005	1064.18	4569.59	3084.80	1507.76	1634.87
3006	219.87	3722.83	2287.90	1267.54	854.95
3008	522.87	4177.86	2556.25	540.90	598.78
3009	1165.07	4202.76	2527.44	649.97	806.50
3010	611	4207.08	2480.83	495.13	563.33
3011	483.21	4175.78	2406.61	443.97	499.53
3012	163.31	4186.13	2487.66	560.05	659.49
3013	1496.21	3990.95	2373.68	704.57	833.33
3014	214.5	4367.89	2609.21	443.05	500.73
3016	99.51	3215.82	1292.85	-8.20	-238.39
3017	86.89	3077.81	1170.21	-99.41	-313.58
3018	145.08	4189.50	2339.81	186.72	161.00
3019	94.45	3782.52	1936.39	-51.94	12.40
3020	70.21	4049.53	2224.48	-115.06	194.03
3021	124.21	3287.14	1369.07	-123.37	-276.66
3022	52.28	3504.74	1591.08	-270.87	-60.12

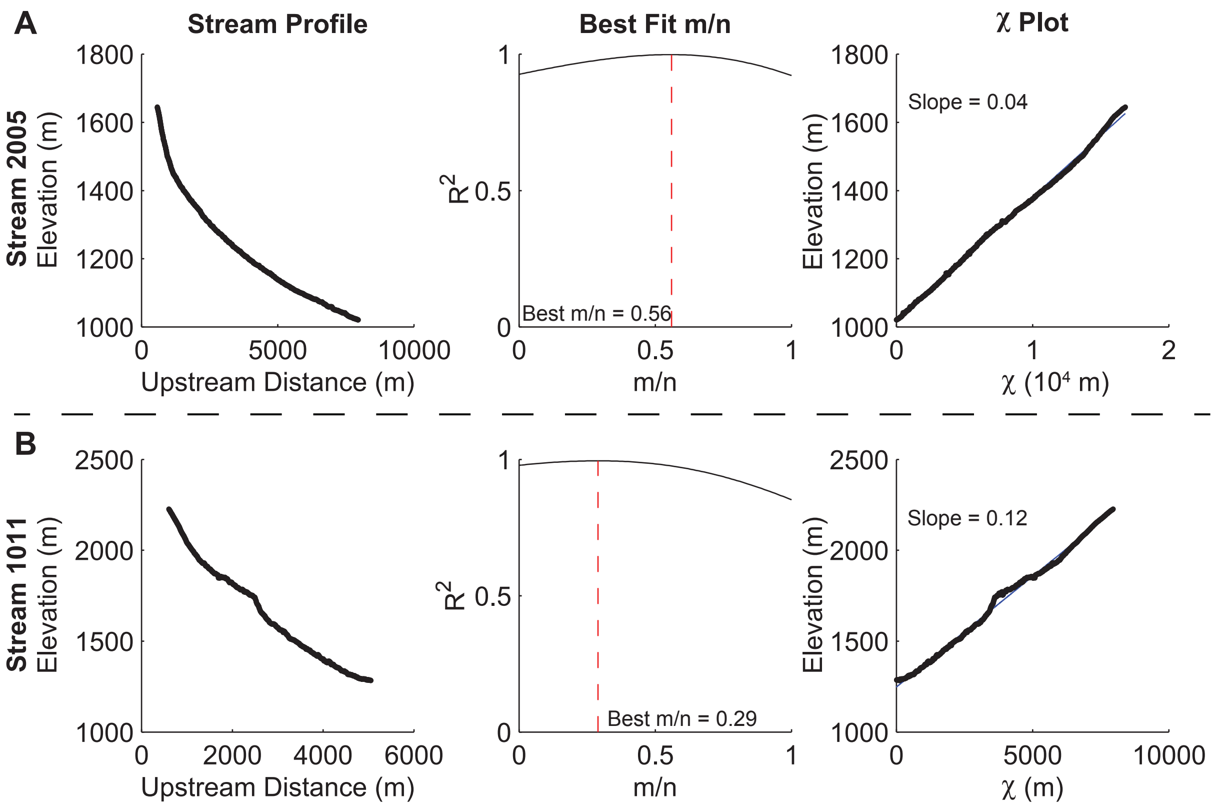

Figure 3: A. Stream profile, best fit m/n plot, and chi plot for stream 2005. B. Stream profile, best fit m/n, and chi plot for stream 1011. The stream profile reveals the knick point in stream 1011. Plots for all of the streams can be found in Appendix A.

best reduced models of erosion rate include the fewest variables while still successfully replacing the full model; the variables in the best reduced models are the primary controllers of erosion rate. The predicted erosion rate is the linear fit model, which is then plotted against the actual erosion rate (Table 4).

Results

In the San Gabriel Mountains, we find erosion rates of 12-1155 m/My for 0.1-170 km^2 catchments. In the San Bernardino Mountains, we find erosion rates of 52-2970 m/My over catchment areas of 0.4-4.2 km^2. As seen in Figure 1, there is a gradient of increasing erosion rate from north to south in the SBM, but no west to east increase in the SGM. In the west and east SGM, erosion rate is highly variable in small catchments but converges to a mean erosion rate, agreeing with Niemi et al. (2005) and Yanites et al. (2009) (Figure 4). As expected, the mean erosion rate for the east SGM is larger than that of the west SGM. All of the catchments in the SBM are small, and therefore highly variable in erosion rate (Figure 4). We find no correlation between erosion rate and catchment elevation (Figures 5). Erosion rate increases with catchment-mean slope until a slope of ~ 30-35^o, consistent with threshold slopes found by DiBiase et al. (2010) and Binnie et al. (2007) (Figure 6).

The linearized stream profiles determine the steepness indices of river profiles, as well as reveal whether streams are transient or steady-state. The SGM and SBM stream profiles were successfully linearized according to the Perron and Royden (2012) methodology (Figure 3A, Appendix A). The channel steepness index, which is the slope of the chi plots, discloses the uplift rate, where higher channel steepness indices correspond with faster uplift rates. Figure 2 reveals a west to east increase in channel steepness in the SGM but no spatial trend within the SBM.

The linear fit models are created to consider catchment metrics and tectonic activity influences on erosion rate. We evaluated whether each variable is significant in predicting erosion rate, and how well

Table 4: Model Parameters and Goodness of Fit.

Model	R^2	Intercept	Area	Minimum Elevation	Maximum Elevation	Range Elevation	Mean Elevation	Mean Slope	Mean $Slope^2$	Centroid Easting	Centroid Northing	Channel Steepness m/n 0.47	Parallel Distance	Perpendicular Distance	log(1/Perpendicular Distance)
Full 1	0.290	50700.0	-1.620	13730	-13730	13730	1.447	-78.170	1.922	0.00159	-0.0128	-1817	0.0128	--	151.3
Full 2	0.217	59210.0	-1.616	17520	-17520	17520	1.262	2.157	-0.001	-0.00145	-0.0154	-1858	0.0147	-0.0132	--
Reduced 1	0.500	2226.0	--	--	--	--	--	--	0.598	--	--	--	0.0099	--	286.8
Reduced 2	0.493	841.5	--	--	--	--	--	-98.970	2.620	--	--	--	0.0150	-0.0270	--

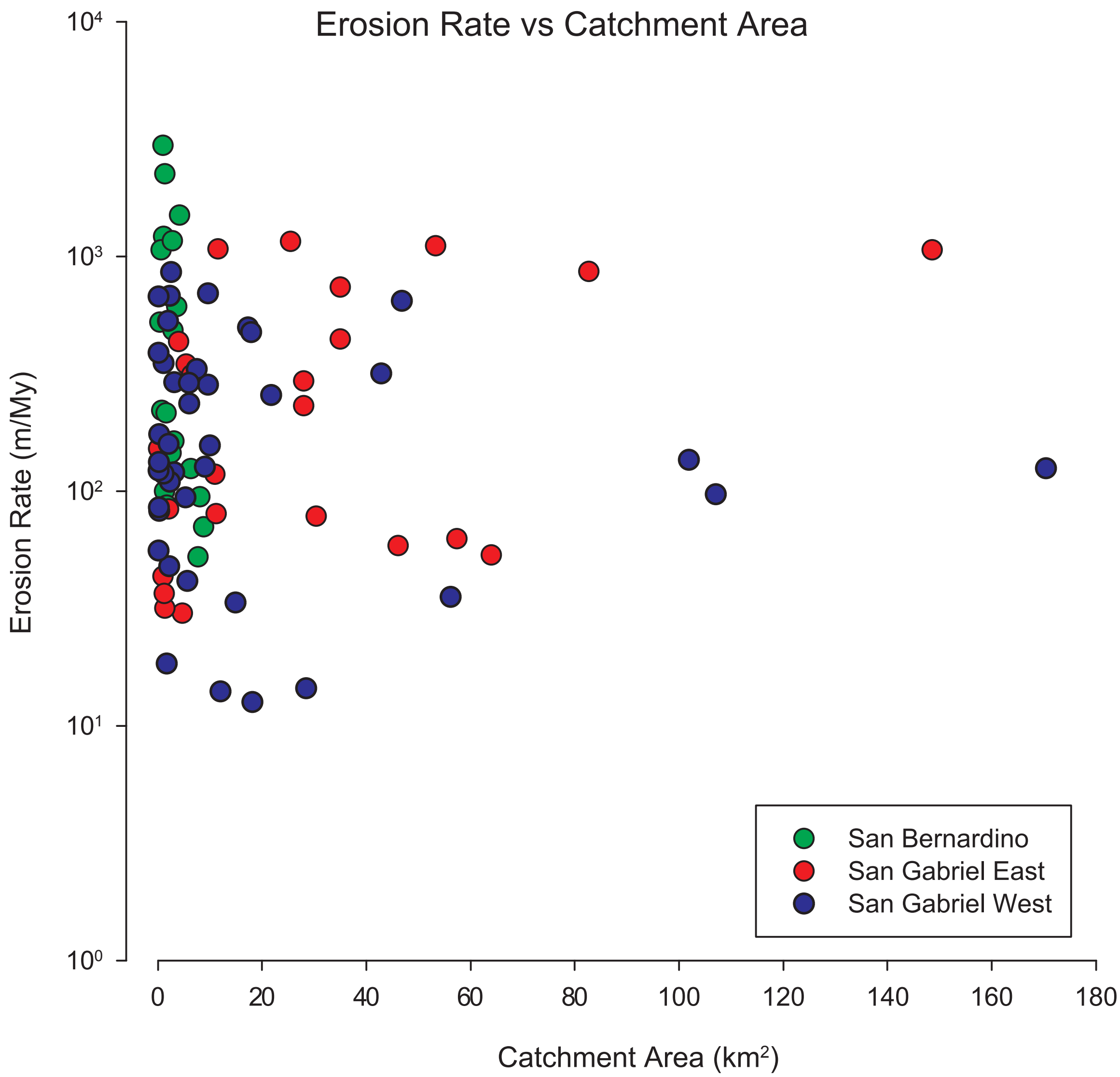

Figure 4: Actual CRN-derived erosion rate (m/My) against catchment area (km2). Data points are colored by catchment location. The plot sho s no clear relation hip between catchment area and erosion rate.

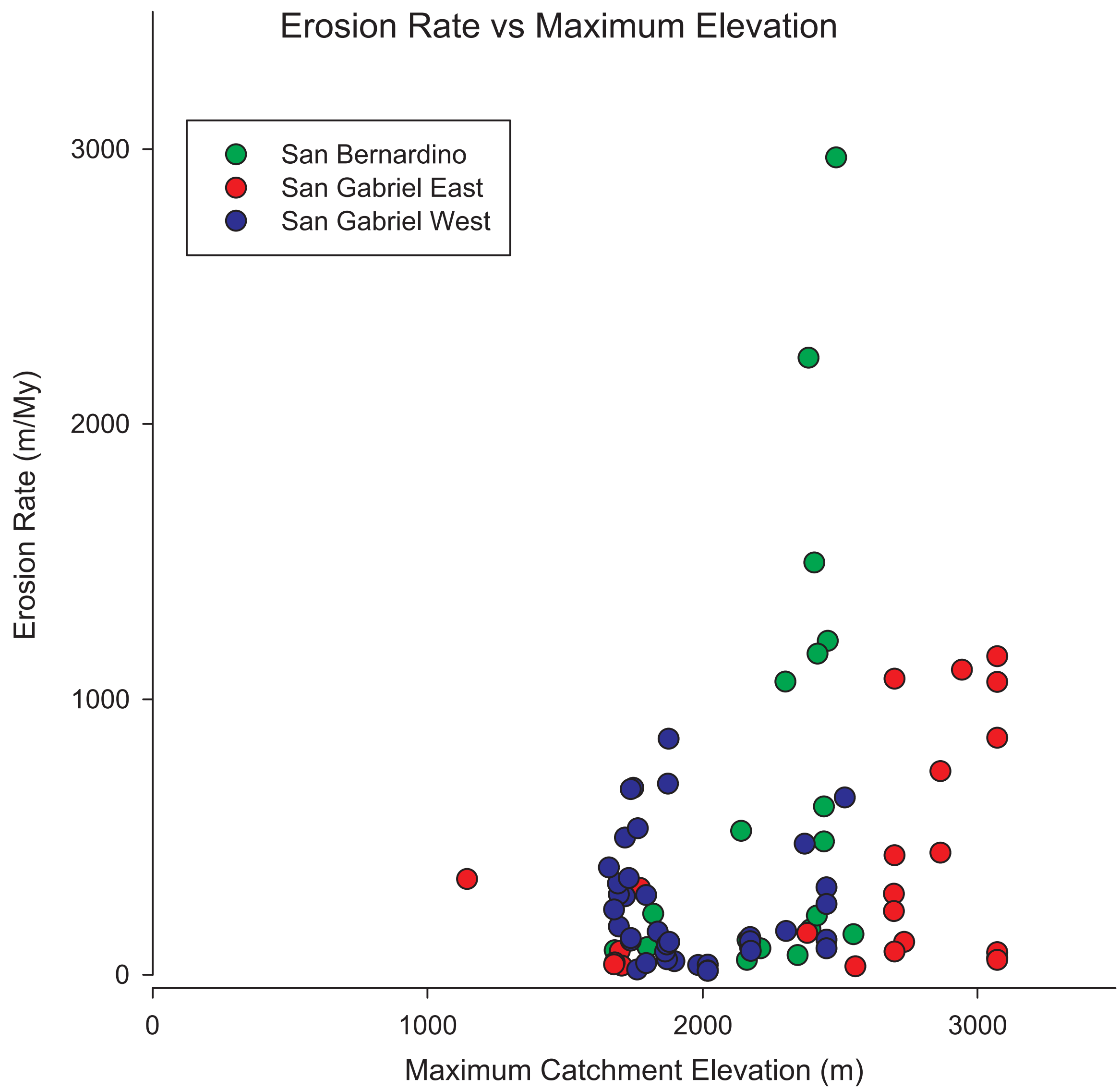

Figure 5: Actual CRN-derived erosion rate (m/My) against maximum catchment elevation (m). Data points are colored by catchment location. The plot shows no clear relation hip between maximum catchment elevation and e osion rate.

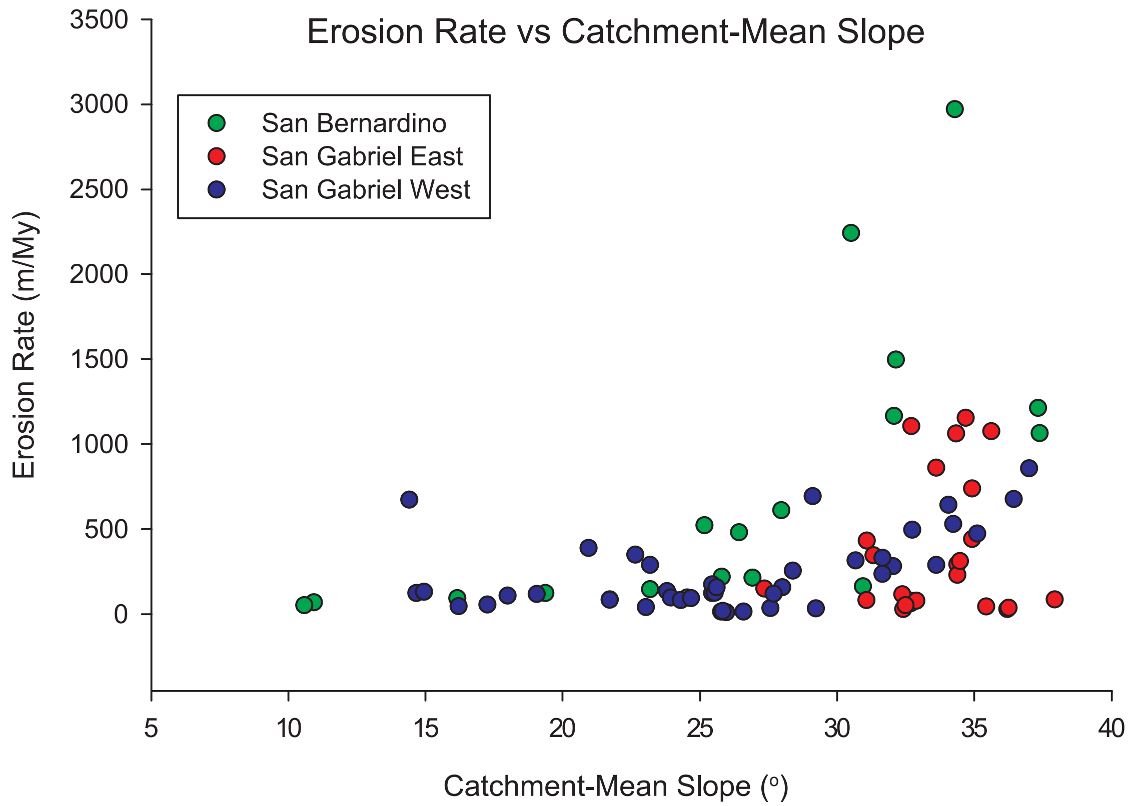

Figure 6: Actual CRN-derived erosion rate (m/My) against catchment-mean slope (°). The posiĀve linear trend between erosion rate and catchment-mean slope decouples at ~30-35o, consistent with threshold slopes found in other studies. Data points are colored by catchment location

we can predict erosion rate from catchment metrics and tectonic activity. For all reduced models, area, elevation, and the centroid latitude and longitude are insignificant in modeling erosion rate, statistically confirming our results from the plots of catchment area and maximum elevation against erosion rate (Figures 4 and 5). None of the reduced models include channel steepness index at m/n 0.38 or 0.47 among the significant variables.

The two best models, reduced model 1 and reduced model 2, have a goodness of fit of 50.0% and 49.3%, respectively. The full models, from which these reduced models came, have goodness of fit values 21.7% and 29.0% (Table 4). With the catchment metrics and tectonic parameters considered in this study, it is possible to only predict 50.0% of erosion rate, at best. Reduced model 1 predicts erosion rate as a function of catchment-mean slope, parallel distance along the SAF, and the log of the inverse of perpendicular distance from the SAF (Figure 7, Table 4). Reduced model 2 predicts erosion rate as a function of catchment-mean slope, catchment-mean slope squared, parallel distance and perpendicular distance from the SAF (Figure 8, Table 4). These two models suggest that the catchment-mean slope and catchment distance from the SAF are the main controls on erosion rates in the SGM and SBM. Both of the reduced models under predict erosion rate for the catchments with high erosion rates (Figures 7 and 8).

Discussion

The CRN-derived erosion rates from this study are in agreement with previously published SGM and SBM erosion rates from CRN, low temperature thermochronometry, and infilling of dams and debris basins. In the SGM, DiBiase et al. (2010) finds CRN-derived erosion rates of 35-1100 m/My, and Niemi et al. (unpub. data) finds 130-1260 m/My. This agrees with the erosion rates inferred from apatite (U-Th)/He thermochronometry and apatite fission track of 110 m/My in the west SGM and 400-1000 m/My in the east SGM (Blythe et al., 2002). Lavé and Burbank (2004) derive erosion rates of 100-140 m/My in

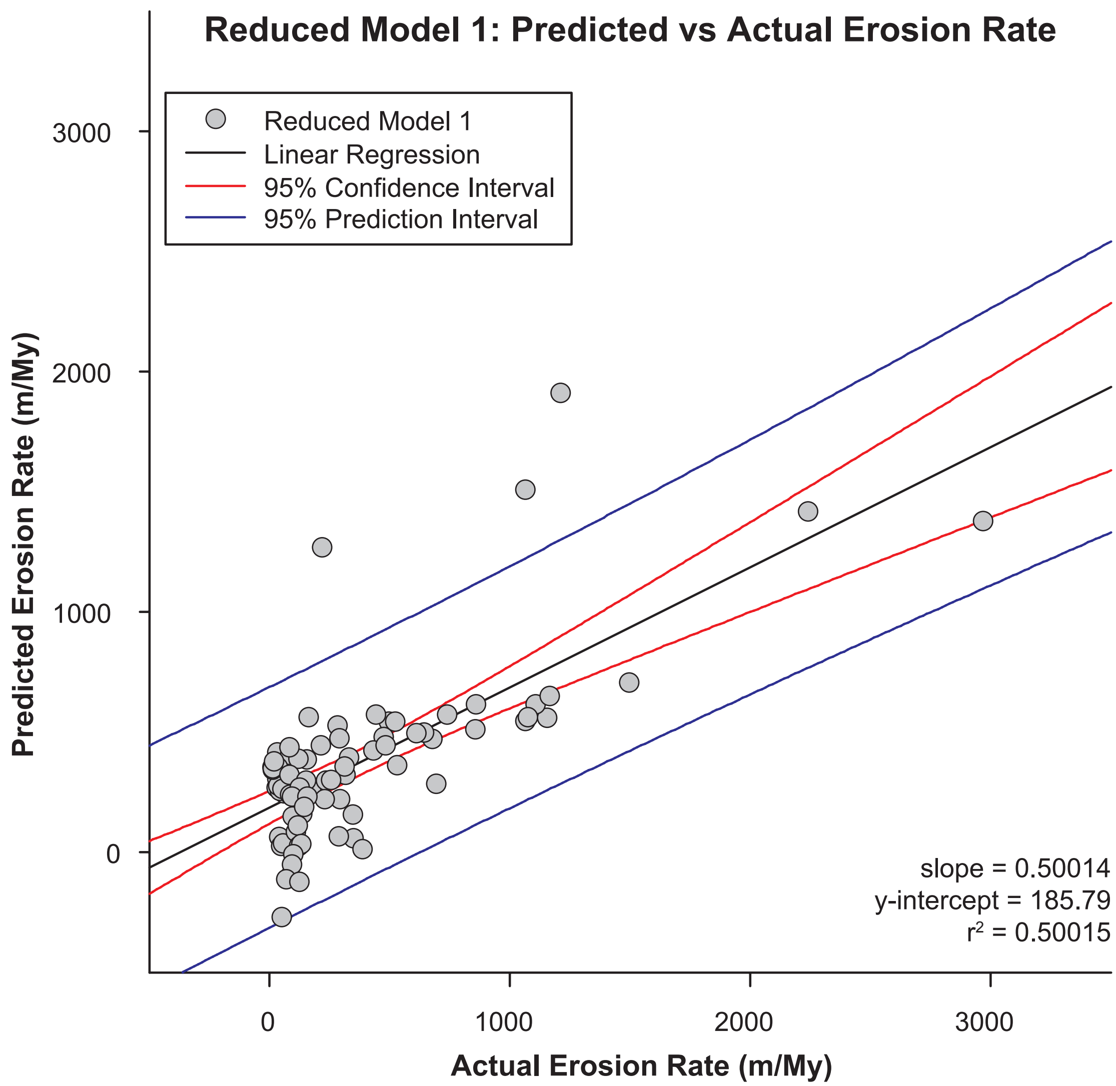

Figure 7: Plot of reduced model 1 predicted against actual erosion rate (m/My). The goodness of fit is 50.0%. The model parameters are listed in Table 4.

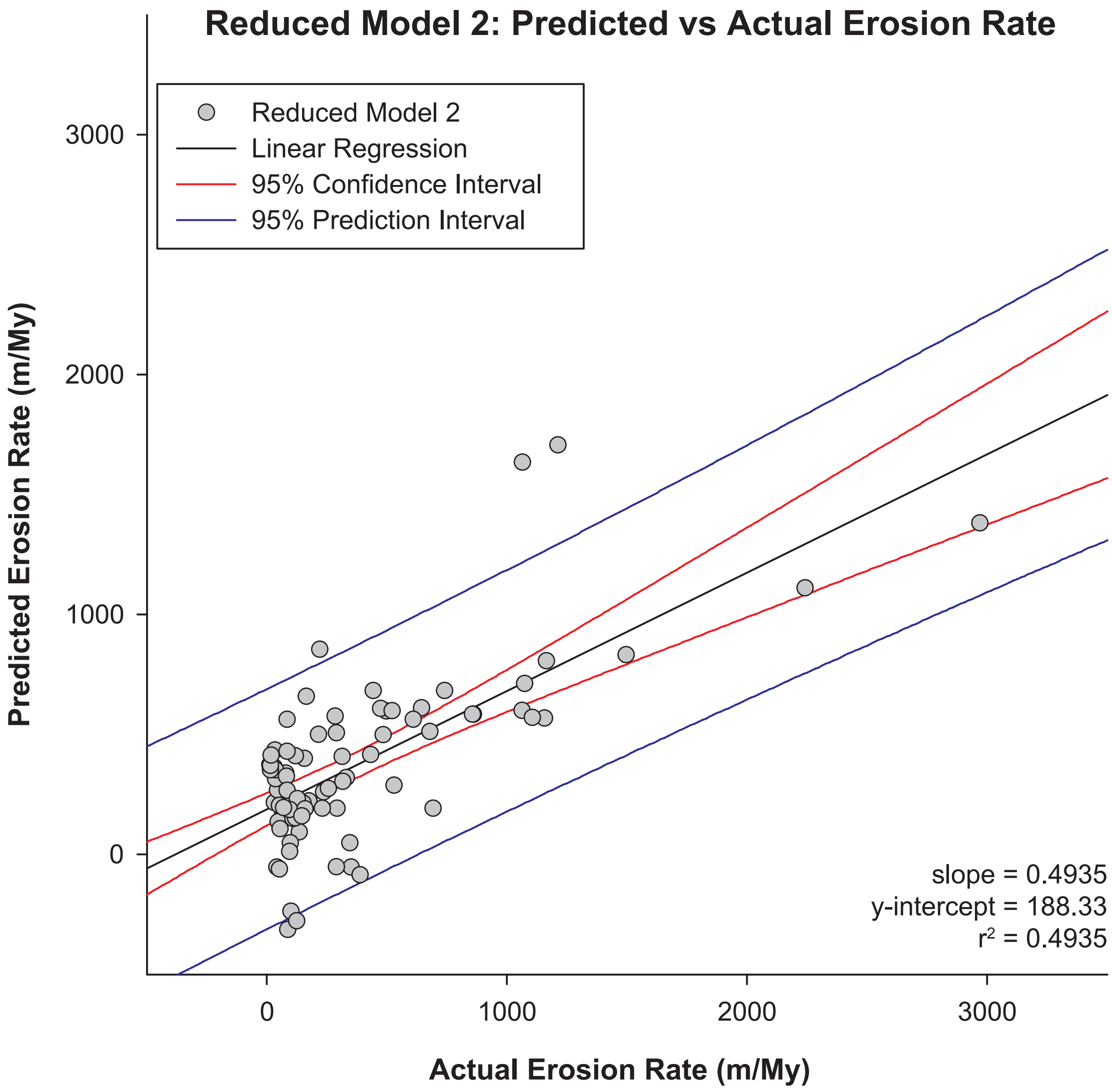

Figure 8: Plot of reduced model 2 predicted against actual erosion rate (m/My). The goodness of fit is 49.3%. The model parameters are listed in Table 4.

the west SGM and 300-800 m/My in the east SGM based on infilling of dams and debris basins. However, Niemi et al. (unpub. data) argues that the Lavé and Burbank (2004) erosion rates underestimate the actual erosion rate due to the unaccounted for effects of wildfires, landslides and soil slumps, chemical weathering, and small sediment size of the samples. In the SBM, Binnie et al. (2007) calculates erosion rates of 52-2700 m/My based on CRN. Using (U-Th)/He and AFT, Spotila et al. (2001) determined the SBM exhumed 3-6 km over 1.5 My, consistent with 2000-4000 m/My erosion rates. In conclusion, the CRN-derived erosion rates presented in this study agree with previously published erosion rates for the SGM and SBM.

Through statistical analysis, we find no correlation between erosion rate and catchment area, which agrees with DiBiase et al. (2010) (Figure 4). Additionally, our results agree with Spotila et al. (2002) that there is no correlation between erosion rate and elevation (Figure 5). Our models indicate that catchment-mean slope is an important parameter affecting erosion rate. One of the two best-fit reduced models includes mean slope as an important parameter, whereas the other does not (Table 4). While our study did not investigate threshold slope, we agree with previous studies that did consider erosion rate and threshold slopes in that slope is an important parameter controlling erosion rate (Spotila et al., 2002; Binnie et al., 2007; DiBiase et al., 2010) (Figure 6). Both the plot of erosion rate against catchment-mean slope and the statistical analyses reveal a significant relationship between erosion rate and catchment-mean slope.

Although channel steepness index increases from west to east in the SGM, it is not a statistically significant parameter in either of the reduced models. This agrees with the results of DiBiase et al. (2010), where channel steepness trends with uplift in the SGM, but the dominance of stochastic mass-wasting events in the SBM makes channel steepness an irrelevant parameter (Figure 2). The Perron and Royden (2012) stream profile transformation makes a few assumptions, such as the spatial homogeneity of uplift rate and erodibility within catchments, and steady-state topography. From the stream profiles and chi plots, the presence of knick points indicates that many of the streams are not in steady-state (Figure 3B). The channel steepness index gradient in the SGM most likely reflects the west to east gradient of increasing uplift; however, Perron and Royden (2012) suggest that channel steepness indices, as shown in chi plots, may reflect parameters such as bedrock erodibility and precipitation, parameters not considered in this study. Finally, many of the chi plots do not appear to accurately represent the stream profile. We hypothesize that this is a result of deep, narrow channels for which the elevation data extracted from the high-resolution DEMs is not consistently reflective of the channel but of the height of the channel walls.

There is a strong correlation between erosion rate and catchment distance from the San Andreas fault. Although Figure 1 reveals a north-south gradient of increasing erosion rate in the SBM, it does not reveal a clear increase in SGM erosion rate from west to east. Nonetheless the statistical analyses reveal the significance of catchment distance from the SAF in predicting erosion rate. The reduced models establish that parallel distance and the perpendicular distance and the log of the inverse of perpendicular distance are necessary parameters in modeling erosion rate. The best fit model includes the log of the inverse of perpendicular distance, designating this perpendicular function as the best approximation of the perpendicular parameter. This study introduces distance from the SAF as a new and essential parameter that influences erosion rates in the SGM and SBM.

With the parameters catchment-mean slope, parallel distance, and a function of perpendicular distance, it is possible to predict ~50% of erosion rate. This study did not evaluate parameters such as precipitation and bedrock erodibility. Stochastic mass-wasting is prominent in the SBM and east SGM, and is implicitly considered in this study because soil production is less than 0.3mm/yr, and therefore any erosion rate higher than this must include mass wasting (Binnie et al., 2010; Niemi et al., unpub. data). While ~50% of erosion is predicted in our models, high erosion rates are significantly under predicted. None of the models were able to resolve the higher erosion rates. However, the results of the study explicitly resolve the significance of catchment-mean slope and seismic shaking from the San Andreas fault, as approximated by distance from and along the fault, in erosion rate in the SGB and SBM.

Conclusion

Statistical analysis of the factors controlling erosion rate in the San Gabriel and San Bernardino Mountains expose catchment area, elevation, and channel steepness index as not important. Seismic shaking from the San Andreas fault, as approximated by catchment distance along and from the fault, and catchment-mean slope are resolved to be the significant erosion rate parameters.

More work is needed to resolve the effects of each proposed erosion rate parameter within and between the San Gabriel and San Bernardino Mountains. In the statistical analysis of erosion parameters, the San Gabriel and San Bernardino Mountains were considered together. However, it is known that the west SGM, east SGM, and SBM are different in uplift and catchment-dominated erosional processes. Statistical analyses considering these three distinct areas could reveal different controls on erosion with variation in uplift and erosional processes. This study did not consider bedrock erodibility, steady-state versus transient rivers, and climatic controls in the statistical analysis and modeling of erosion rate, which future work could consider. Additionally, our channel steepness results indicate that channel steepness may correlate with erosion rate and uplift and exhumation trends in the San Gabriel Mountains. Further study in this area may reveal a defined relationship between these parameters. In addition, channel steepness is hypothesized to only be a controlling erosion rate factor in catchments not dominated by stochastic mass-wasting events. The identification and investigation of these catchments would advance understanding of channel steepness as an erosion parameter both universally and within the San Gabriel and San Bernardino Mountains.

In conclusion, this study finds catchment-mean slope and seismic shaking, as approximated by distance from the SAF, to be the significant parameters controlling erosion rate. Yet additional research of all erosion rate parameters is necessary to conclusively resolve their contribution to erosion rate in both within the San Gabriel and San Bernardino Mountains and in the broader context of orogenesis and landscape formation.

References

Binnie, S. A., Phillips, W. M., Summerfield, M. A., & Fifield, L. K. (2007). Tectonic uplift, threshold hillslopes, and denudation rates in a developing mountain range. *Geology*, *35*(8), 743-746.

Binnie, S. A., Phillips, W. M., Summerfield, M. A., Fifield, L. K., & Spotila, J. A. (2008). Patterns of denudation through time in the San Bernardino Mountains, California: Implications for early-stage orogenesis. *Earth and Planetary Science Letters*, *276*(1), 62-72.

Binnie, S. A., Phillips, W. M., Summerfield, M. A., Fifield, L. K., & Spotila, J. A. (2010). Tectonic and climatic controls of denudation rates in active orogens: The San Bernardino Mountains, California. *Geomorphology*, *118*(3), 249-261.

Blythe, A. E., Burbank, D. W., Farley, K. A., & Fielding, E. J. (2000). Structural and topographic evolution of the central Transverse Ranges, California, from apatite fission-track, (U-Th)/He and digital elevation model analyses. *Basin Research*, *12*(2), 97-114.

Blythe, A. E., House, M. A., & Spotila, J. A. (2002). Low-temperature thermochronology of the San Gabriel and San Bernardino Mountains, southern California: Constraining structural evolution. *Special Papers-Geological Society of America*, 231-250.

DiBiase, R. A., Whipple, K. X., Heimsath, A. M., & Ouimet, W. B. (2010). Landscape form and millennial erosion rates in the San Gabriel Mountains, CA. *Earth and Planetary Science Letters*, *289*(1), 134-144.

Duvall, A., Kirby, E., & Burbank, D. (2004). Tectonic and lithologic controls on bedrock channel profiles and processes in coastal California. *Journal of Geophysical Research: Earth Surface (2003–2012)*, *109*(F3).

Granger, D. E., Kirchner, J. W., & Finkel, R. (1996). Spatially averaged long-term erosion rates measured from in situ-produced cosmogenic nuclides in alluvial sediment. *The Journal of Geology*, 249-257.

Lavé, J., & Burbank, D. (2004). Denudation processes and rates in the Transverse Ranges, southern California: Erosional response of a transitional landscape to external and anthropogenic forcing. *Journal of Geophysical Research: Earth Surface (2003–2012)*, *109*(F1).

Lechler, A. R., & Niemi, N. A. (2012). The influence of snow sublimation on the isotopic composition of spring and surface waters in the southwestern United States: Implications for stable isotope–based paleoaltimetry and hydrologic studies. *Geological Society of America Bulletin*, *124*(3-4), 318-334.

Minnich, R. A. (1986). Snow levels and amounts in the mountains of southern California. *Journal of Hydrology*, *89*(1), 37-58.

Meunier, P., Uchida, T., & Hovius, N. (2013). Landslide patterns reveal the sources of large earthquakes. *Earth and Planetary Science Letters*, *363*, 27-33.

Niemi, N. A., Binnie, S. A., Burbank, D. W., Stewart, P. H., & Freeman, T. (unpub. data). Variability in ^{10}Be-drived denudation rates from the San Gabriel Mountains, California.

Niemi, N. A., Oskin, M., Burbank, D. W., Heimsath, A. M., & Gabet, E. J. (2005). Effects of bedrock landslides on cosmogenically determined erosion rates. *Earth and Planetary Science Letters*, *237*(3), 480-498.

Nourse, J. A. (2002). Middle Miocene reconstruction of the central and eastern San Gabriel Mountains, southern California, with implications for evolution of the San Gabriel fault and Los Angeles basin. *Special Papers-Geological Society of America*, 161-186.

Ouimet, W. B. (2010). Landslides associated with the May 12, 2008 Wenchuan earthquake: implications for the erosion and tectonic evolution of the Longmen Shan. *Tectonophysics*, *491*(1), 244-252.

Perron, J. T., & Royden, L. (2012). An integral approach to bedrock river profile analysis. *Earth Surface Processes and Landforms*, *38*(6), 570-576.

Powell, R. E., & Weldon, R. J. (1992). Evolution of the San Andreas fault. *Annual Review of Earth and Planetary Sciences*, *20*, 431.

Schildgen, T. F., Phillips, W. M., & Purves, R. S. (2005). Simulation of snow shielding corrections for cosmogenic nuclide surface exposure studies. *Geomorphology*, *64*(1), 67-85.

Spotila, J. A., Farley, K. A., Yule, J. D., & Reiners, P. W. (2001). Near-field transpressive deformation along the San Andreas fault zone in southern California, based on exhumation constrained by (U-Th)/He dating. *Journal of Geophysical Research*, *106*(B12), 30909-30.

Spotila, J. A., House, M. A., Blythe, A. E., Niemi, N. A., & Bank, G. C. (2002). Controls on the erosion and geomorphic evolution of the San Bernardino and San Gabriel Mountains, southern California. *Special Papers-Geological Society of America*, 205-230.

Walls, C., Rockwell, T., Mueller, K., Bock, Y., Williams, S., Pfanner, J., Dolan, J., & Fang, P. (1998). Escape tectonics in the Los Angeles metropolitan region and implications for seismic risk. *Nature*, *394*(6691), 356-360.

Wobus, C., Whipple, K. X., Kirby, E., Snyder, N., Johnson, J., Spyropolou, K., Crosby, B., & Sheehan, D. (2006). Tectonics from topography: Procedures, promise, and pitfalls. *Special Papers-Geological Society of America*, *398*, 55.

Yanites, B. J., Tucker, G. E., & Anderson, R. S. (2009). Numerical and analytical models of cosmogenic radionuclide dynamics in landslide-dominated drainage basins. *Journal of Geophysical Research: Earth Surface (2003–2012)*, *114*(F1).

Appendix

Appendix A: Stream Profiles, Best Fit m/n Plots, Chi Plots

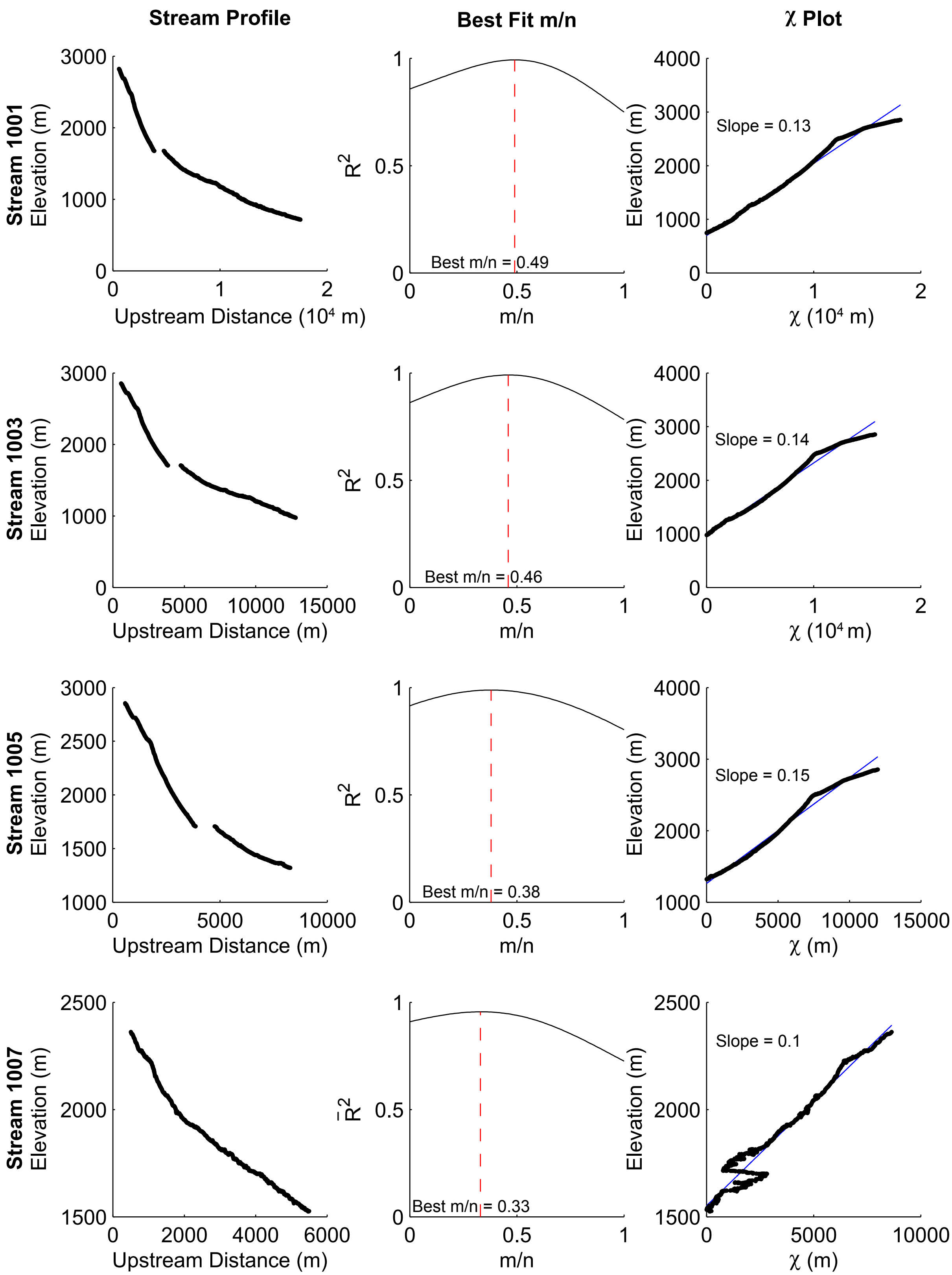

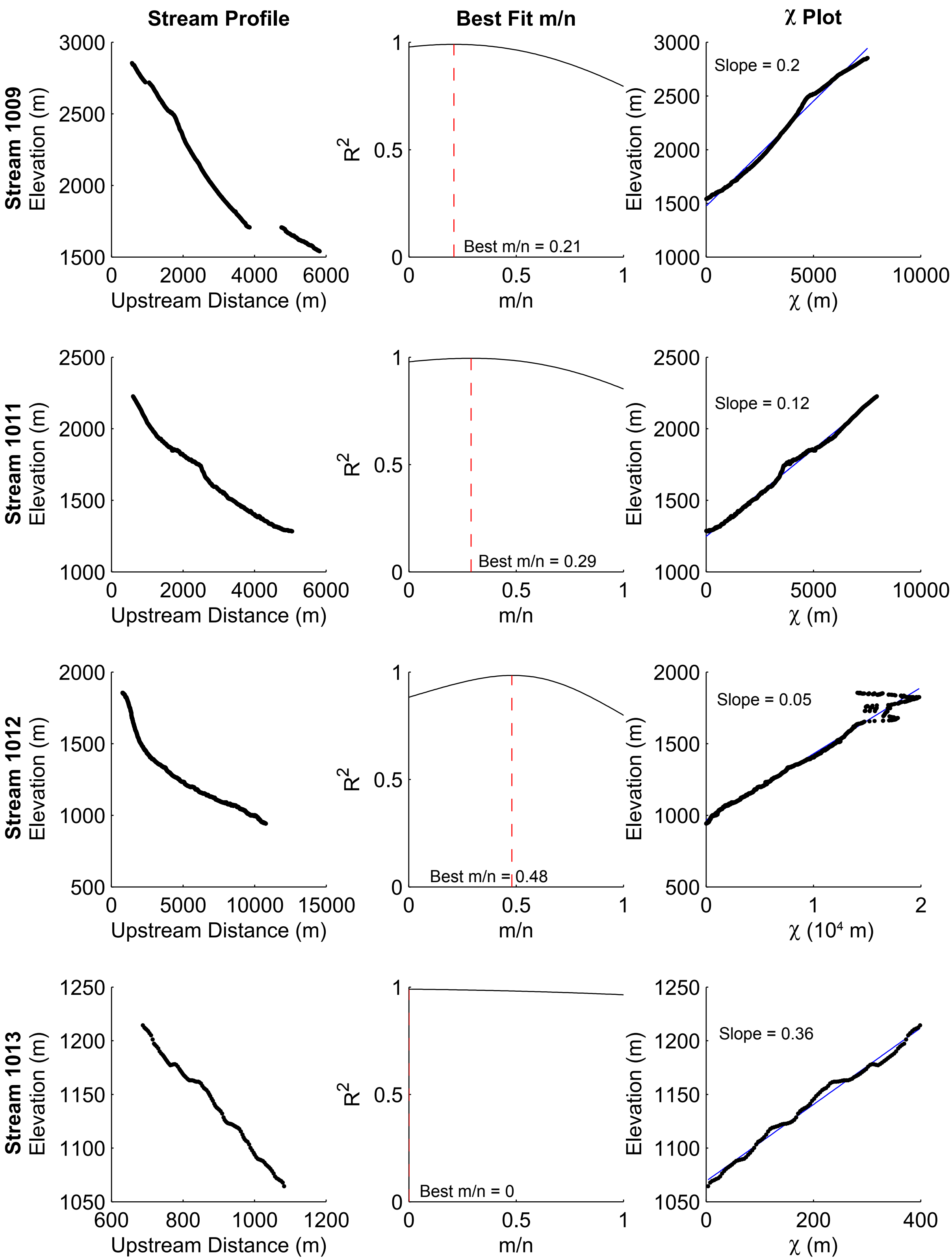
Stream Profile
Best Fit m/n
χ Plot
Stream 1009
Stream 1011
Stream 1012
Stream 1013
Elevation (m)
Upstream Distance (m)
R2
m/n
χ (m)
χ (10⁴ m)
Best m/n = 0.21
Best m/n = 0.29
Best m/n = 0.48
Best m/n = 0
Slope = 0.2
Slope = 0.12
Slope = 0.05
Slope = 0.36

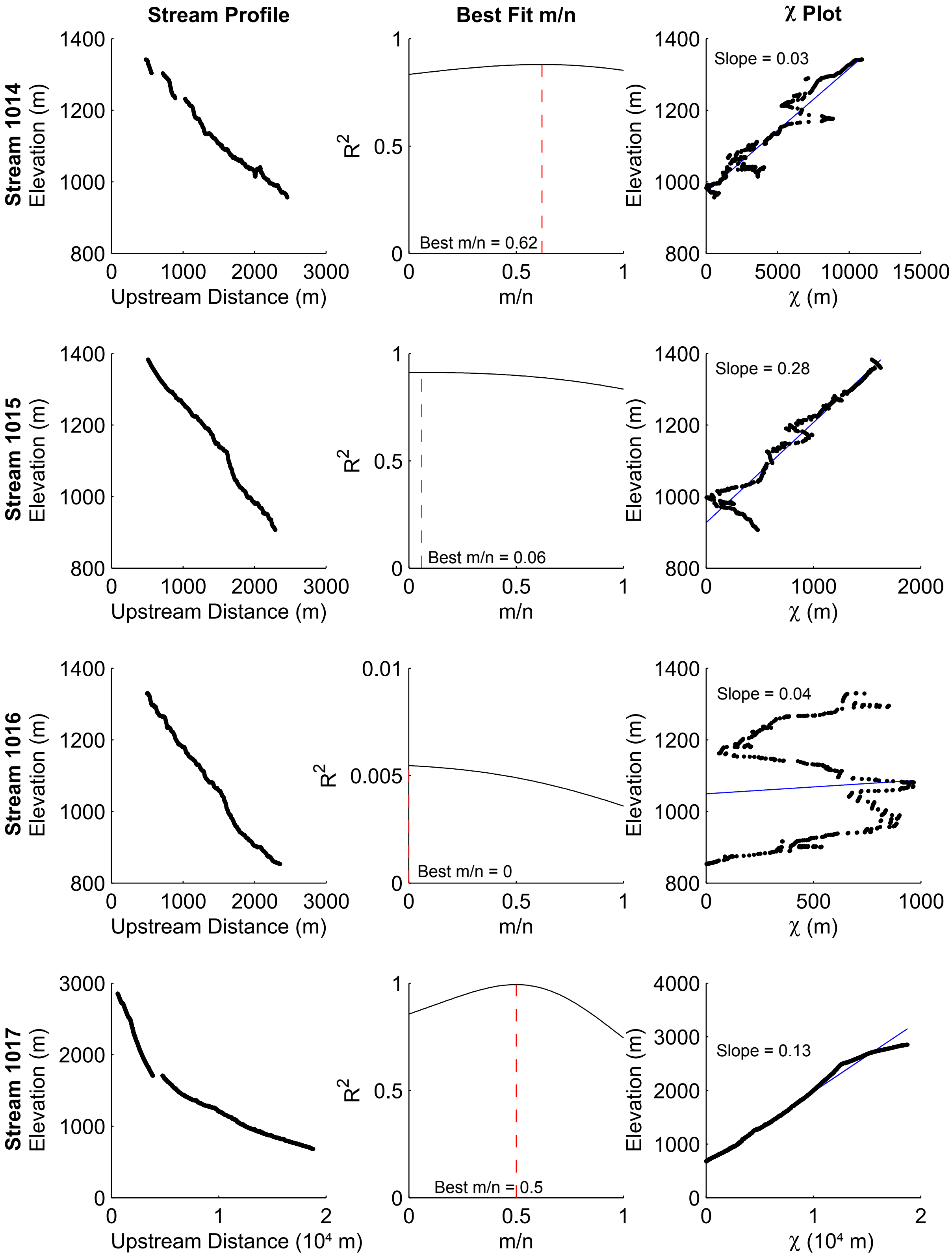
Stream Profile
Best Fit m/n
χ Plot
Stream 1014
Elevation (m)
Upstream Distance (m)
R^2
Best m/n = 0.62
m/n
Slope = 0.03
χ (m)
Stream 1015
Best m/n = 0.06
Slope = 0.28
Stream 1016
Best m/n = 0
Slope = 0.04
Stream 1017
Upstream Distance (10⁴ m)
Best m/n = 0.5
Slope = 0.13
χ (10⁴ m)

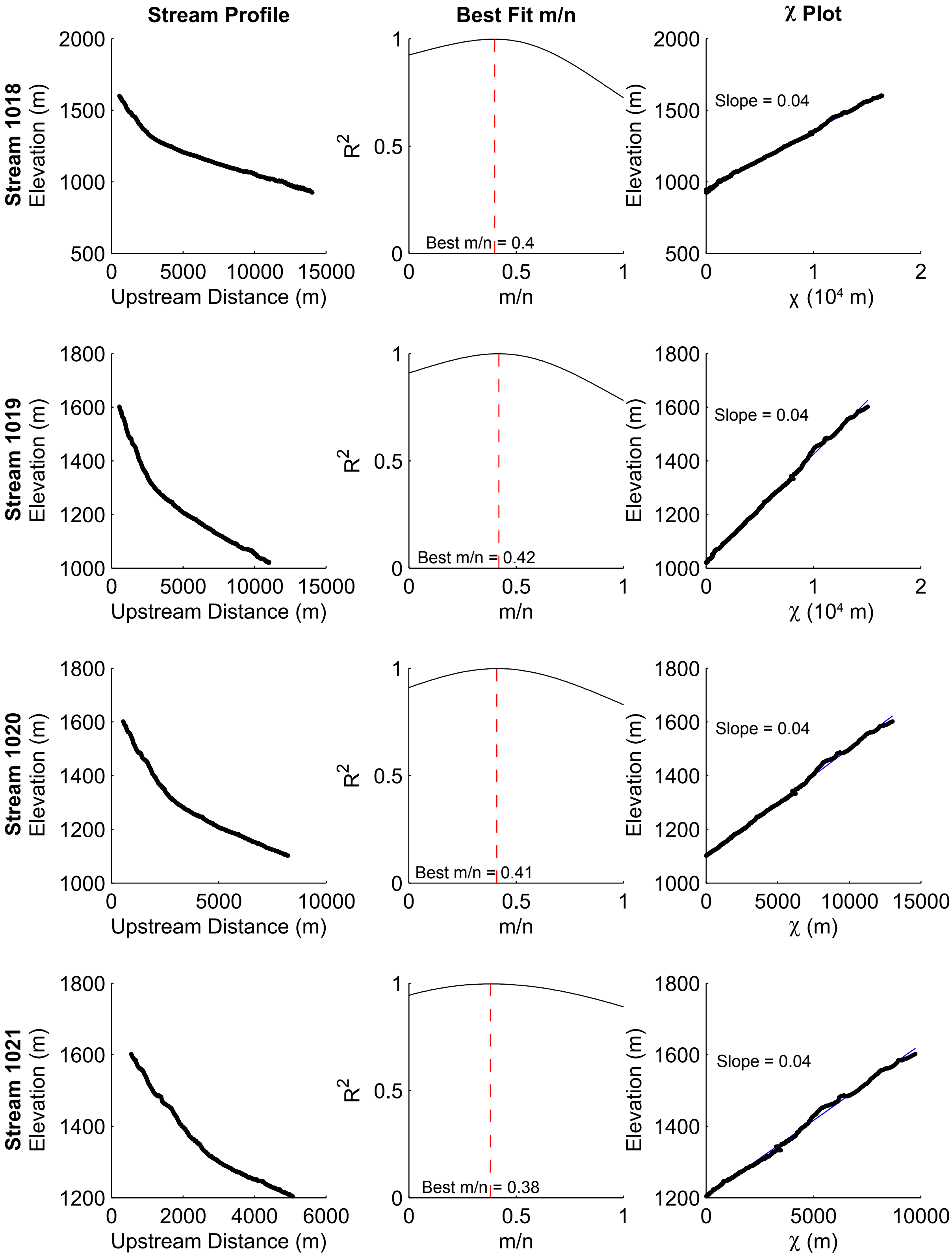
Stream Profile
Best Fit m/n
χ Plot
Stream 1018
Stream 1019
Stream 1020
Stream 1021
Elevation (m)
Upstream Distance (m)
R^2
m/n
Best m/n = 0.4
Best m/n = 0.42
Best m/n = 0.41
Best m/n = 0.38
Slope = 0.04
χ (10⁴ m)
χ (m)

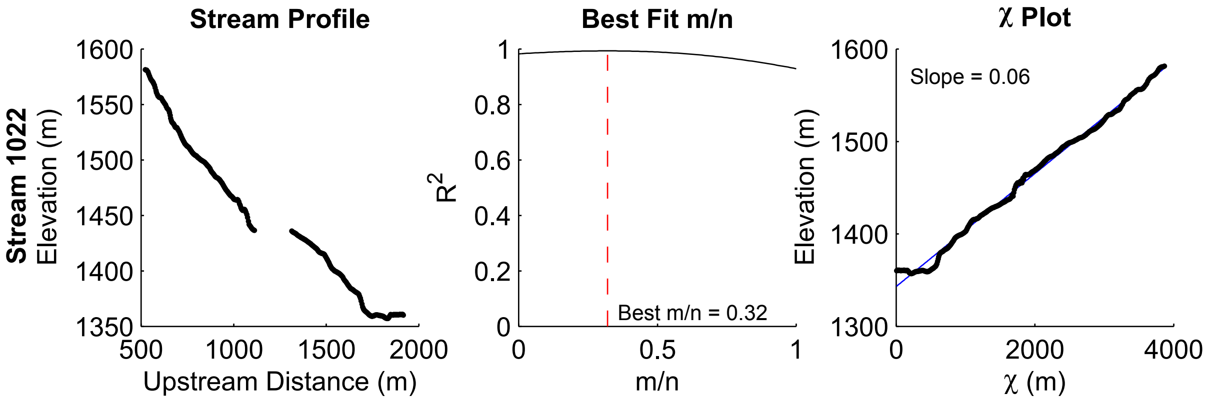
Stream Profile
Stream 1022
Elevation (m)
1600
1550
1500
1450
1400
1350
500
1000
1500
2000
Upstream Distance (m)
Best Fit m/n
R^2
1
0.8
0.6
0.4
0.2
0
0.5
Best m/n = 0.32
m/n
χ Plot
Slope = 0.06
Elevation (m)
1600
1500
1400
1300
0
2000
4000
χ (m)

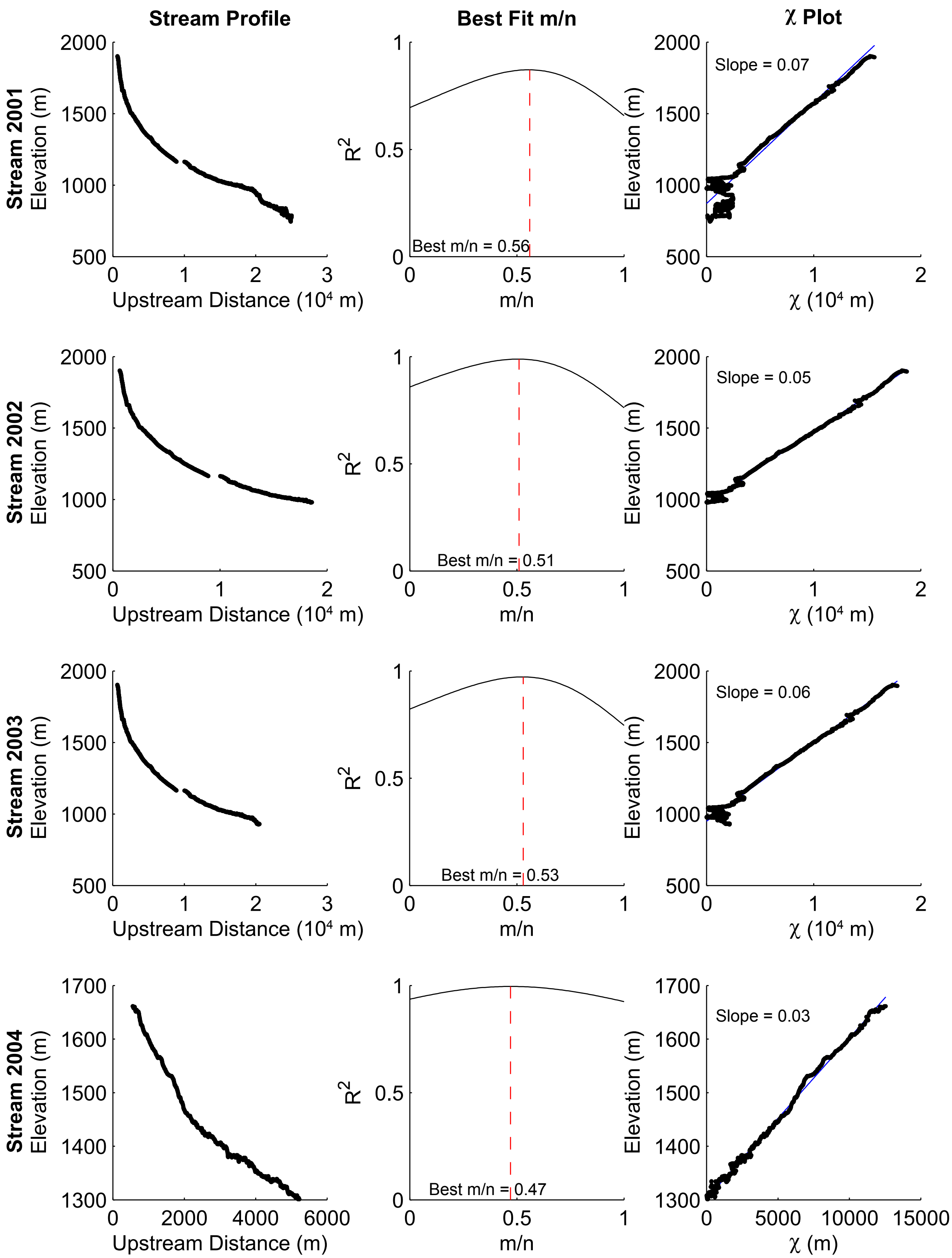

Stream Profile
Best Fit m/n
χ Plot
Stream 2001
Stream 2002
Stream 2003
Stream 2004
Elevation (m)
Upstream Distance (10⁴ m)
Upstream Distance (m)
R²
m/n
χ (10⁴ m)
χ (m)
Best m/n = 0.56
Best m/n = 0.51
Best m/n = 0.53
Best m/n = 0.47
Slope = 0.07
Slope = 0.05
Slope = 0.06
Slope = 0.03

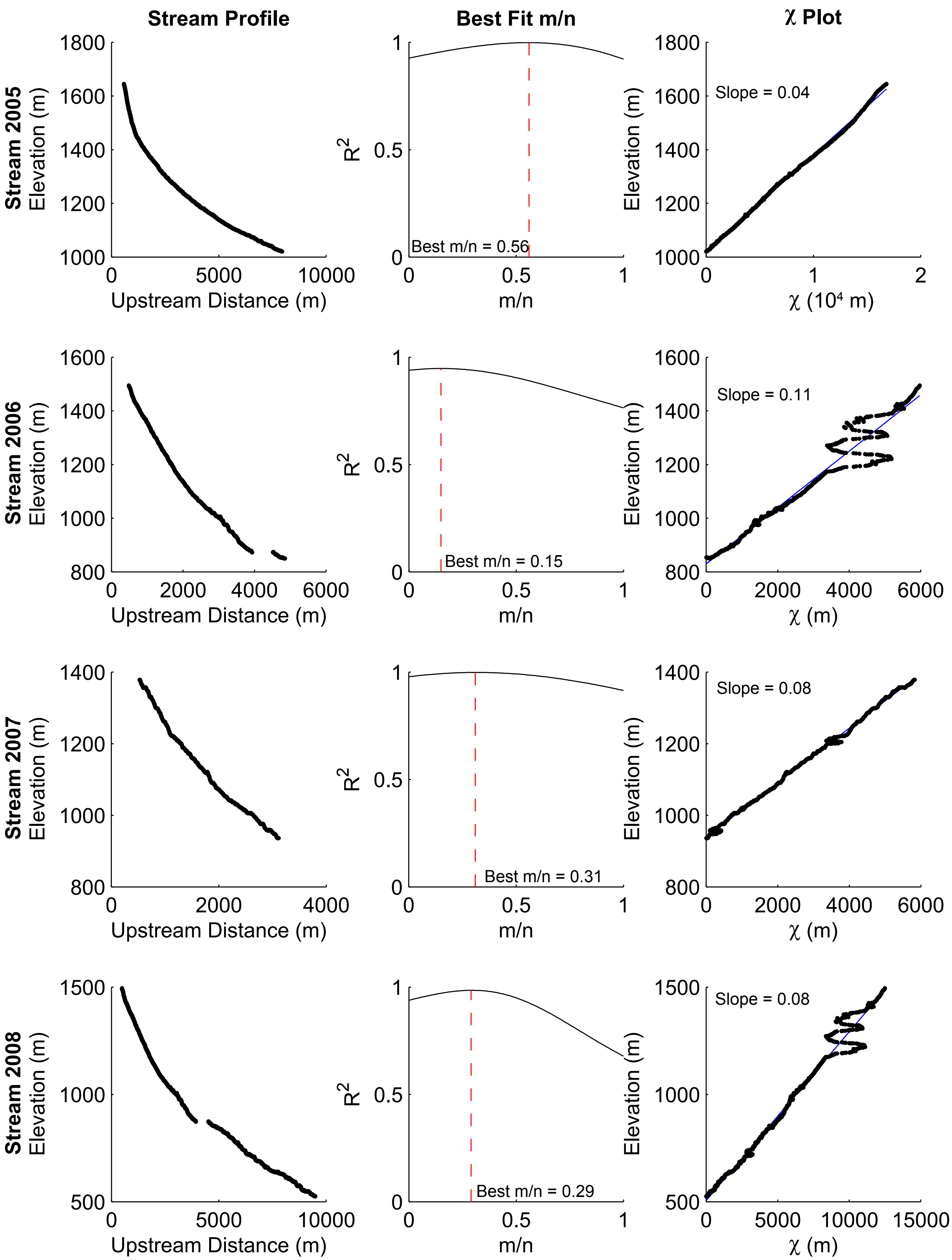
Stream Profile
Best Fit m/n
χ Plot
Stream 2005
Stream 2006
Stream 2007
Stream 2008
Elevation (m)
Upstream Distance (m)
R^2
m/n
χ (10^4 m)
χ (m)
Best m/n = 0.56
Best m/n = 0.15
Best m/n = 0.31
Best m/n = 0.29
Slope = 0.04
Slope = 0.11
Slope = 0.08
Slope = 0.08

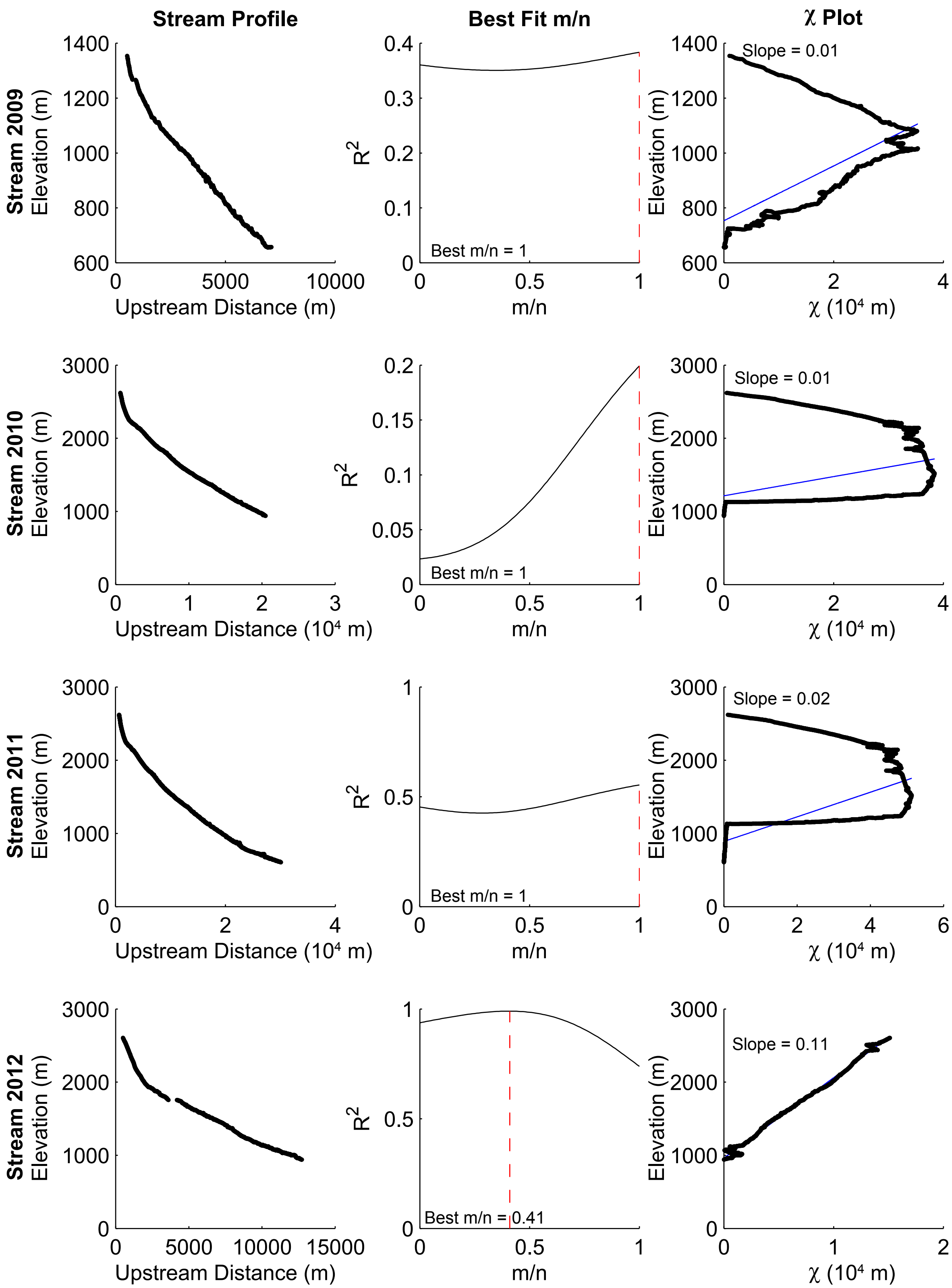
Stream Profile
Best Fit m/n
χ Plot
Stream 2009
Stream 2010
Stream 2011
Stream 2012
Elevation (m)
Upstream Distance (m)
Upstream Distance (10⁴ m)
R^2
m/n
χ (10⁴ m)
Best m/n = 1
Best m/n = 1
Best m/n = 1
Best m/n = 0.41
Slope = 0.01
Slope = 0.01
Slope = 0.02
Slope = 0.11

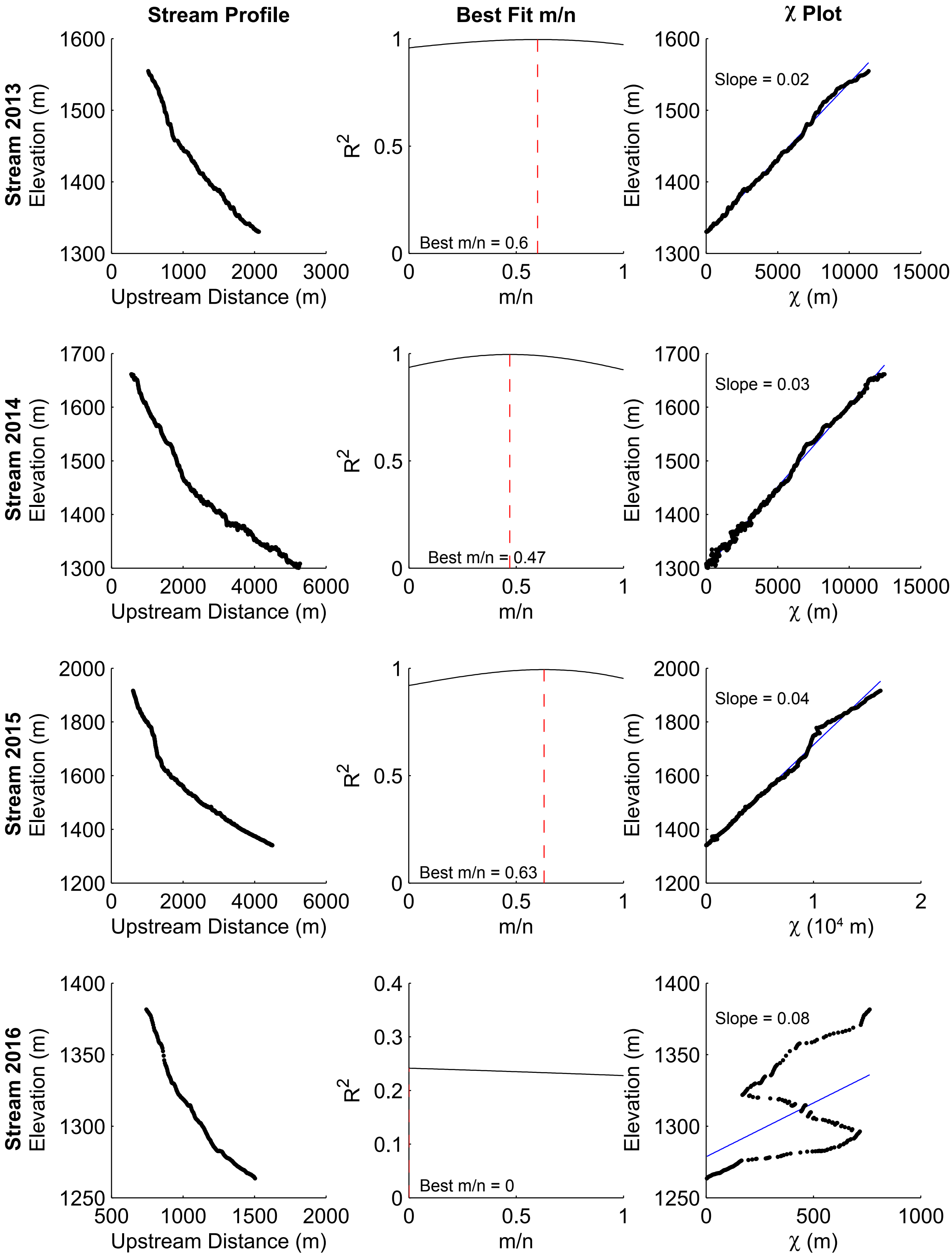
Stream Profile
Best Fit m/n
χ Plot
Stream 2013
Stream 2014
Stream 2015
Stream 2016
Elevation (m)
Upstream Distance (m)
R^2
m/n
χ (m)
χ (10^4 m)
Best m/n = 0.6
Best m/n = 0.47
Best m/n = 0.63
Best m/n = 0
Slope = 0.02
Slope = 0.03
Slope = 0.04
Slope = 0.08

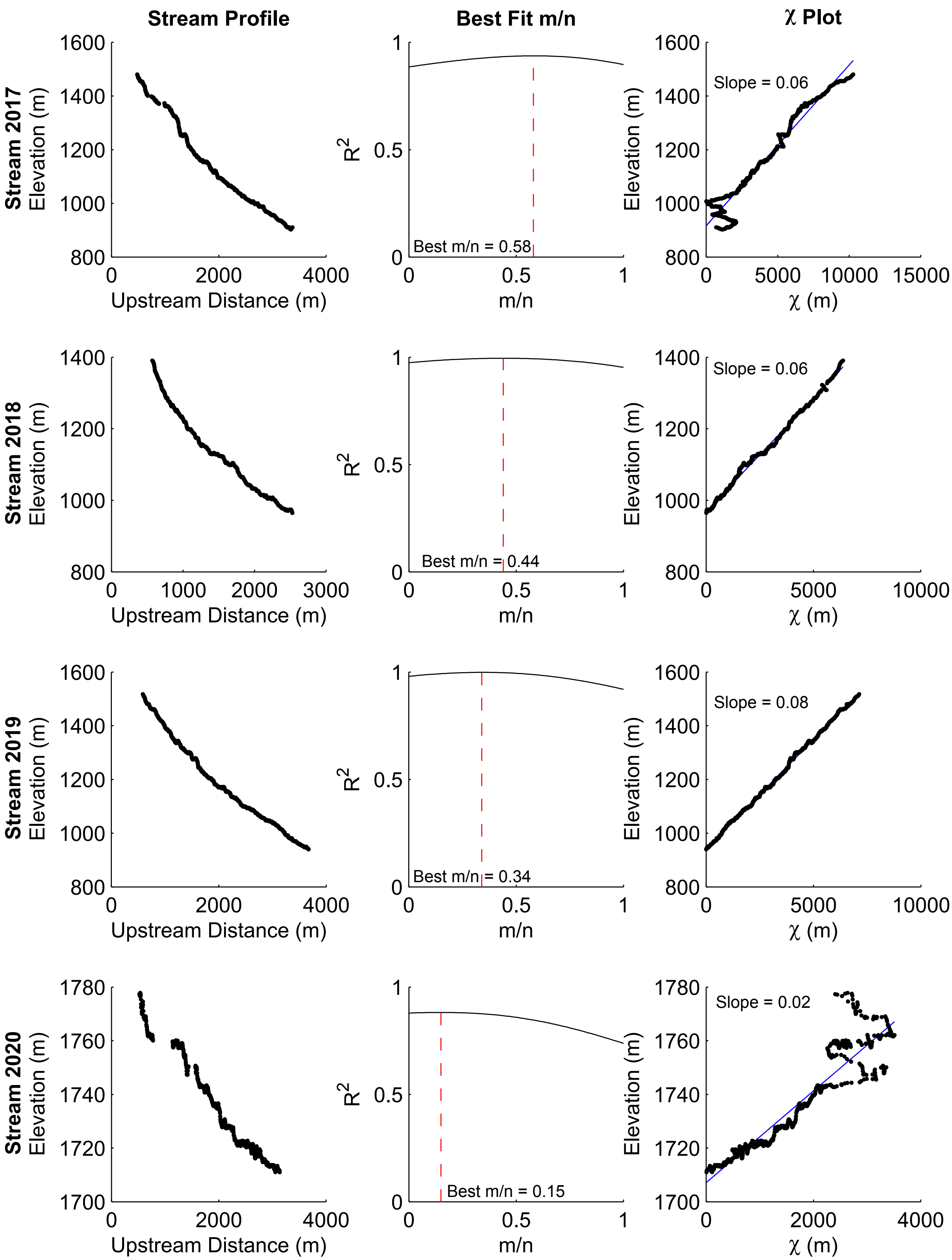
Stream Profile
Best Fit m/n
χ Plot
Stream 2017
Stream 2018
Stream 2019
Stream 2020
Elevation (m)
Upstream Distance (m)
R^2
m/n
χ (m)
Best m/n = 0.58
Best m/n = 0.44
Best m/n = 0.34
Best m/n = 0.15
Slope = 0.06
Slope = 0.06
Slope = 0.08
Slope = 0.02

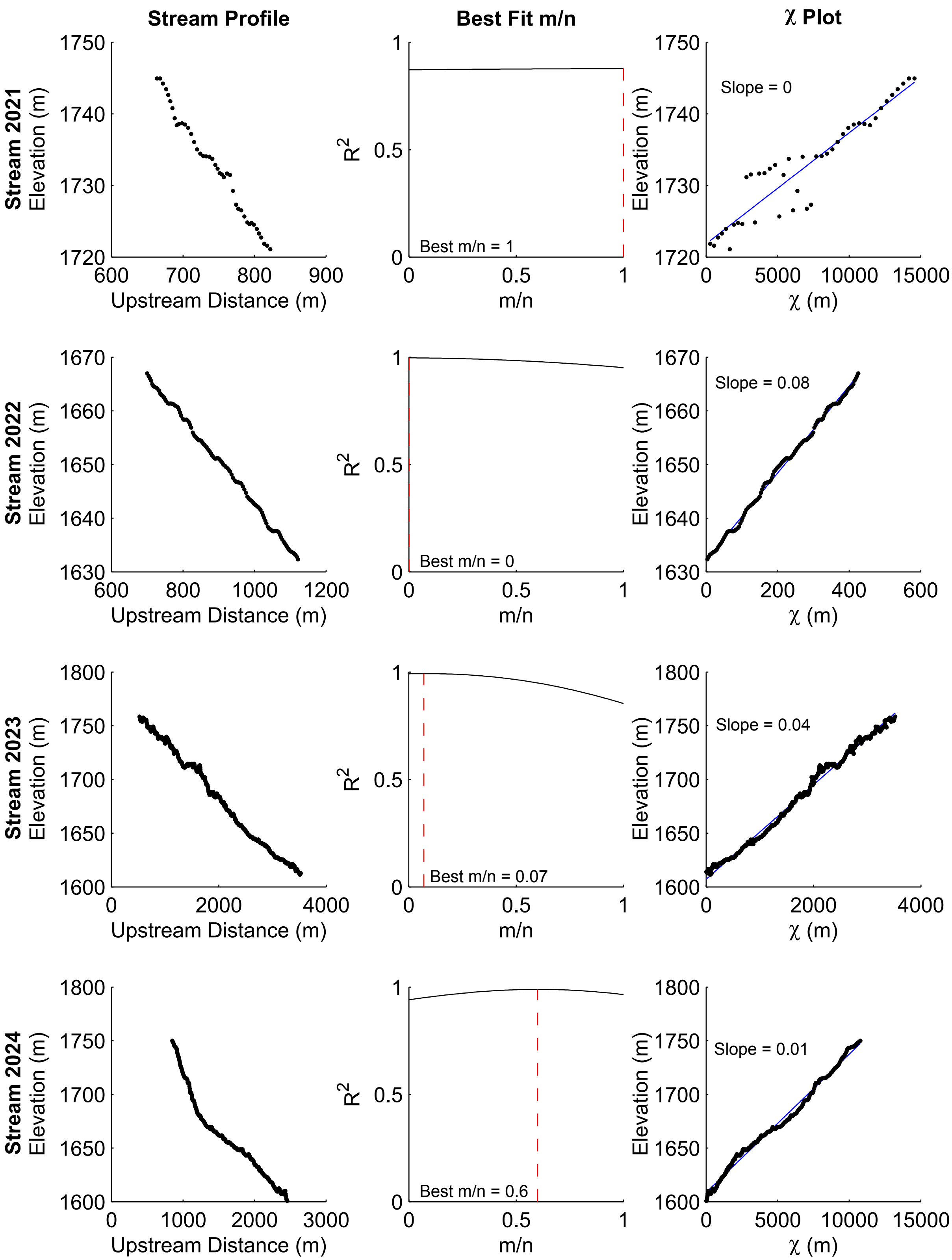
Stream Profile
Best Fit m/n
χ Plot
Stream 2021
Stream 2022
Stream 2023
Stream 2024
Elevation (m)
Upstream Distance (m)
R^2
m/n
χ (m)
Best m/n = 1
Best m/n = 0
Best m/n = 0.07
Best m/n = 0.6
Slope = 0
Slope = 0.08
Slope = 0.04
Slope = 0.01

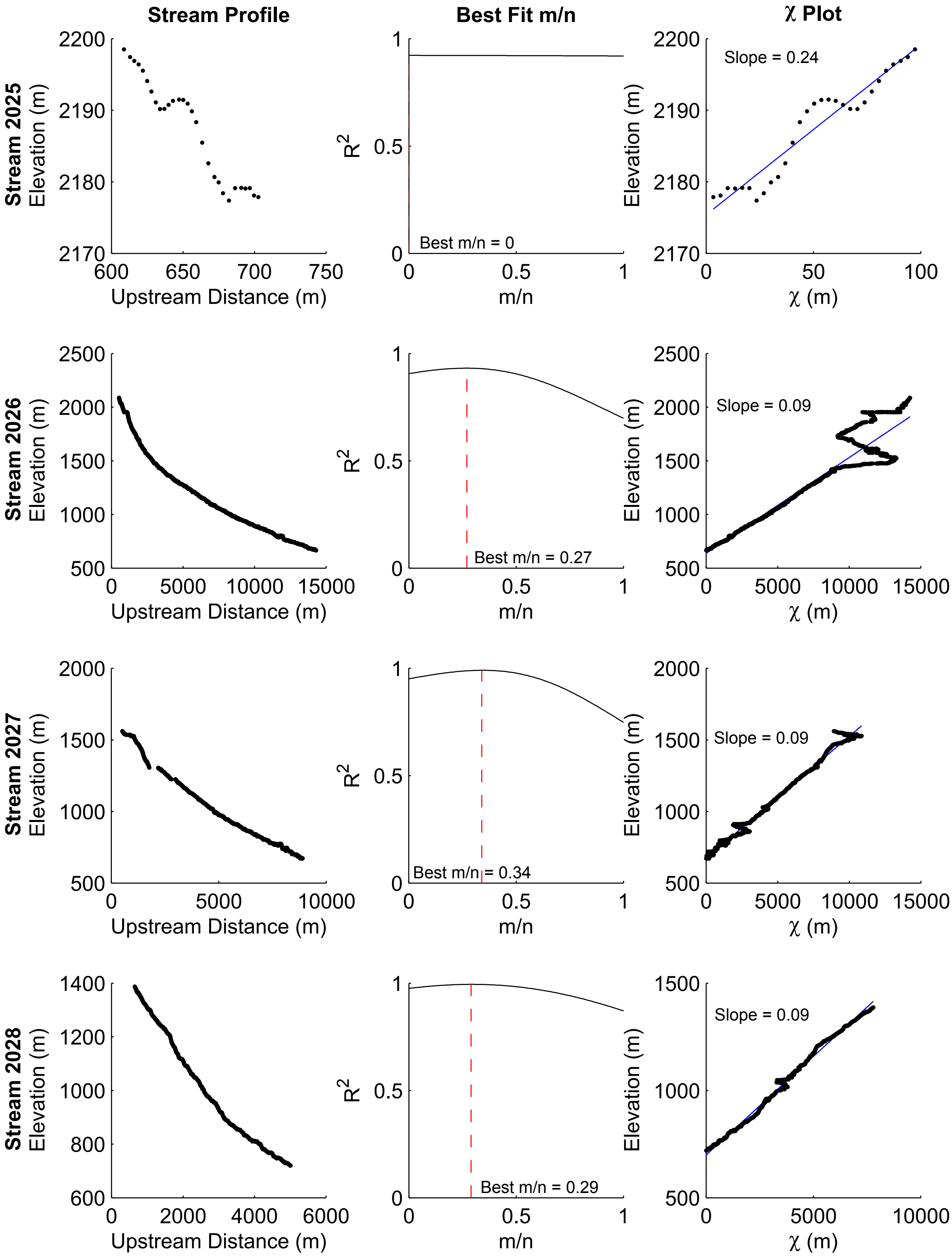
Stream Profile
Best Fit m/n
χ Plot
Stream 2025
Elevation (m)
Upstream Distance (m)
R^2
m/n
Best m/n = 0
Slope = 0.24
χ (m)
Stream 2026
Best m/n = 0.27
Slope = 0.09
Stream 2027
Best m/n = 0.34
Slope = 0.09
Stream 2028
Best m/n = 0.29
Slope = 0.09

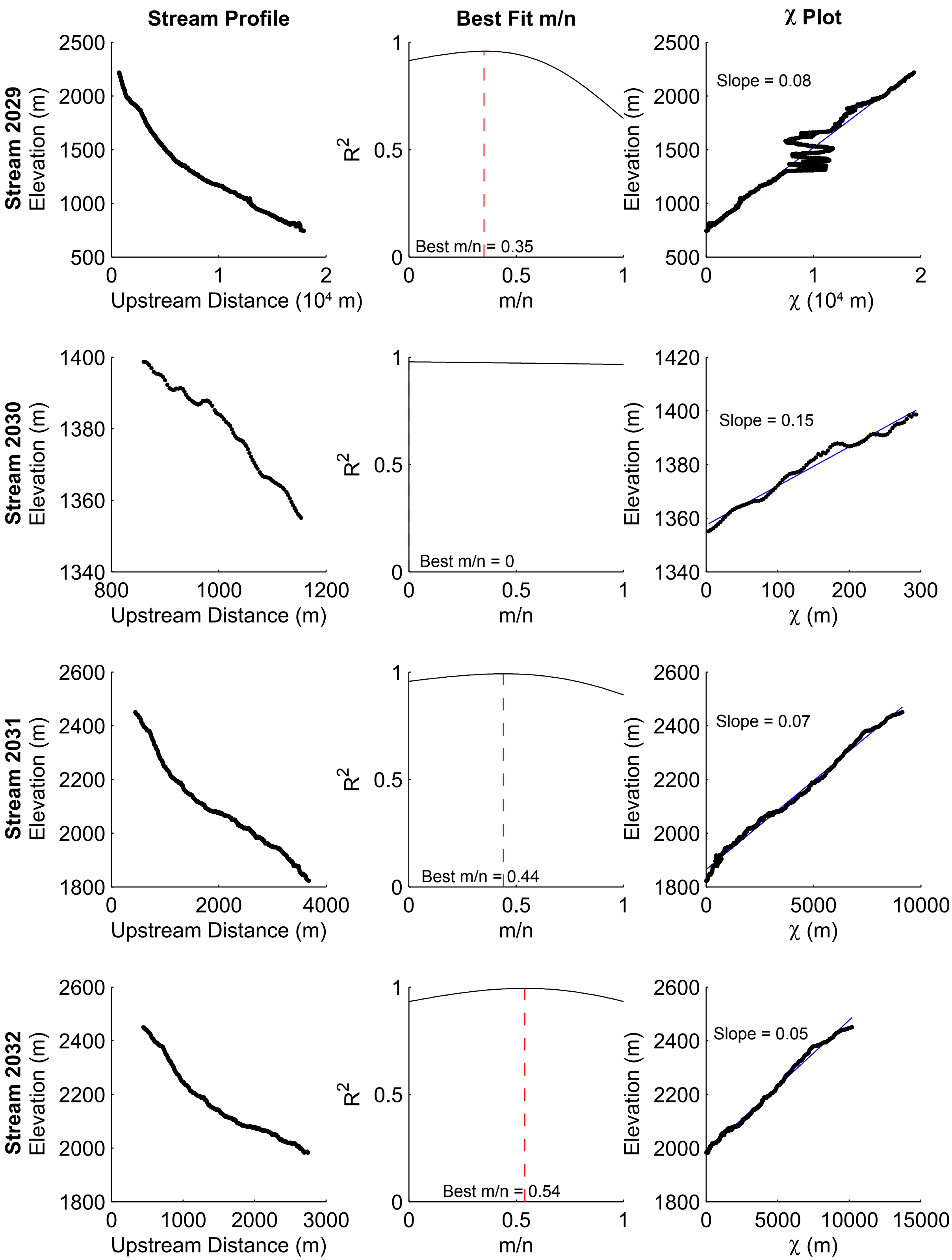
Stream Profile
Best Fit m/n
χ Plot
Stream 2029
Elevation (m)
Upstream Distance (10⁴ m)
R^2
m/n
Best m/n = 0.35
Slope = 0.08
χ (10⁴ m)
Stream 2030
Upstream Distance (m)
Best m/n = 0
Slope = 0.15
χ (m)
Stream 2031
Best m/n = 0.44
Slope = 0.07
Stream 2032
Best m/n = 0.54
Slope = 0.05

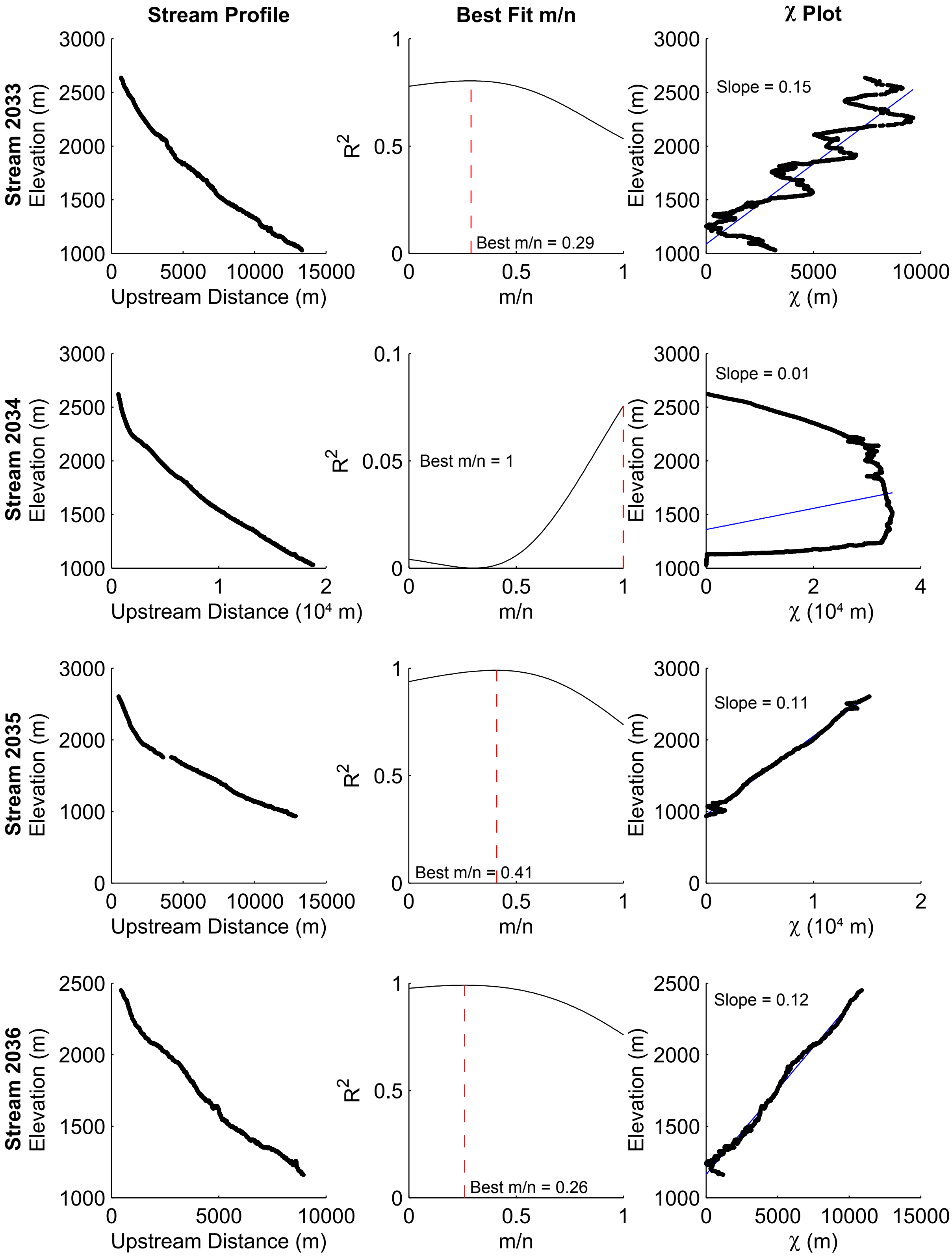

Stream Profile
Best Fit m/n
χ Plot
Stream 2033
Stream 2034
Stream 2035
Stream 2036
Elevation (m)
Upstream Distance (m)
Upstream Distance (10⁴ m)
R²
m/n
χ (m)
χ (10⁴ m)
Best m/n = 0.29
Best m/n = 1
Best m/n = 0.41
Best m/n = 0.26
Slope = 0.15
Slope = 0.01
Slope = 0.11
Slope = 0.12

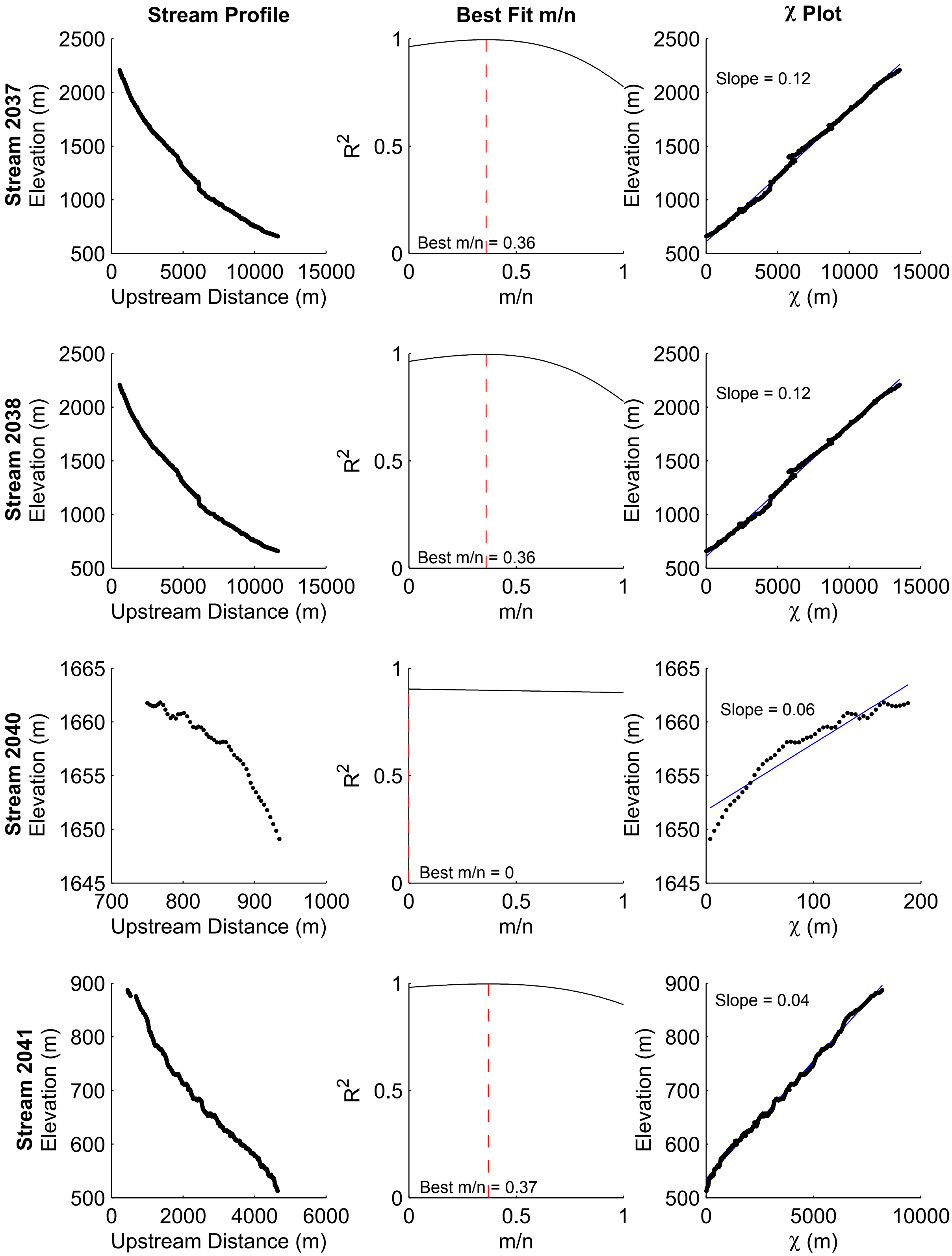
Stream Profile
Best Fit m/n
χ Plot
Stream 2037
Stream 2038
Stream 2040
Stream 2041
Elevation (m)
Upstream Distance (m)
R^2
m/n
χ (m)
Best m/n = 0.36
Best m/n = 0.36
Best m/n = 0
Best m/n = 0.37
Slope = 0.12
Slope = 0.12
Slope = 0.06
Slope = 0.04

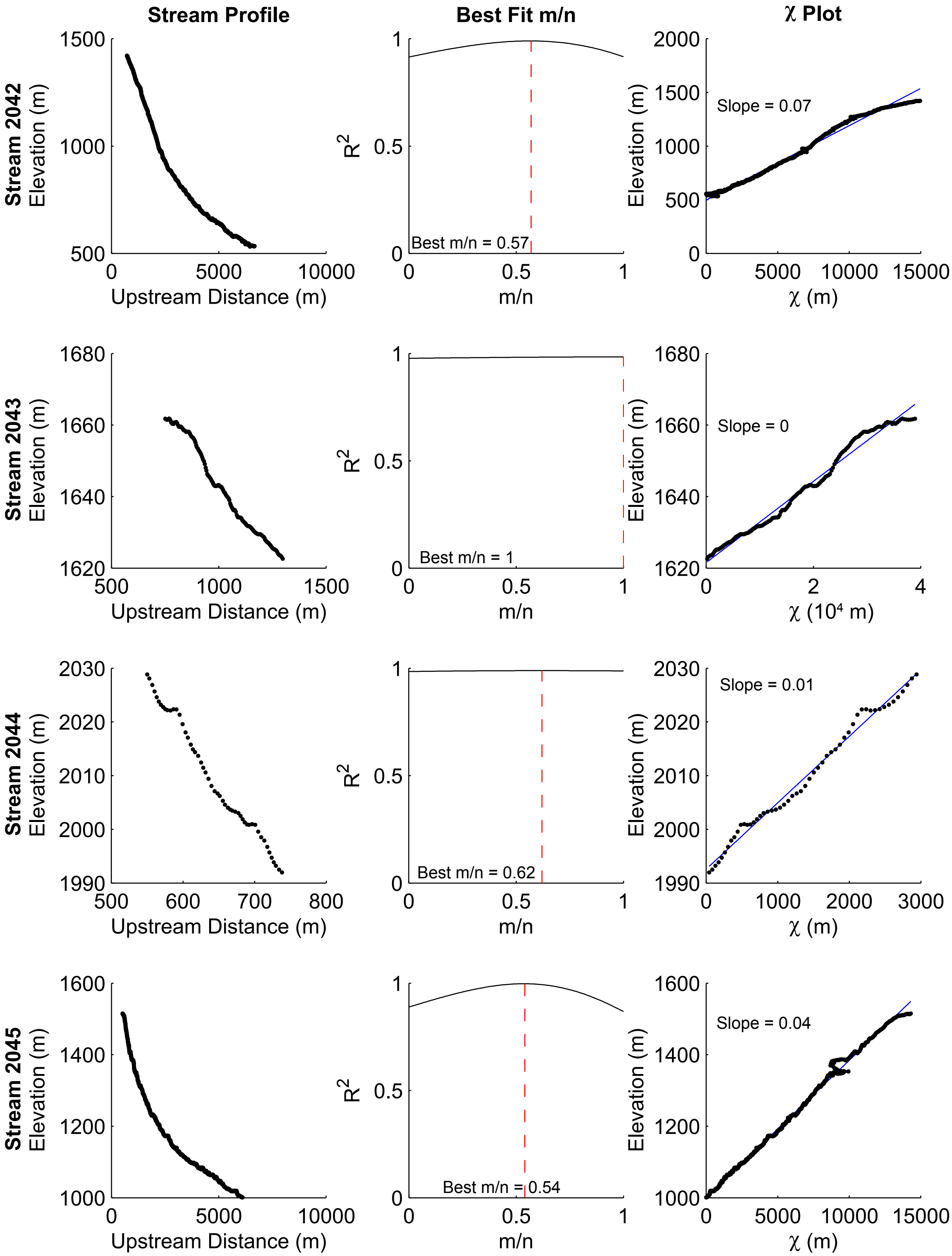
Stream Profile
Best Fit m/n
χ Plot
Stream 2042
Elevation (m)
Upstream Distance (m)
R^2
m/n
Best m/n = 0.57
Slope = 0.07
χ (m)
Stream 2043
Best m/n = 1
Slope = 0
χ (10^4 m)
Stream 2044
Best m/n = 0.62
Slope = 0.01
Stream 2045
Best m/n = 0.54
Slope = 0.04

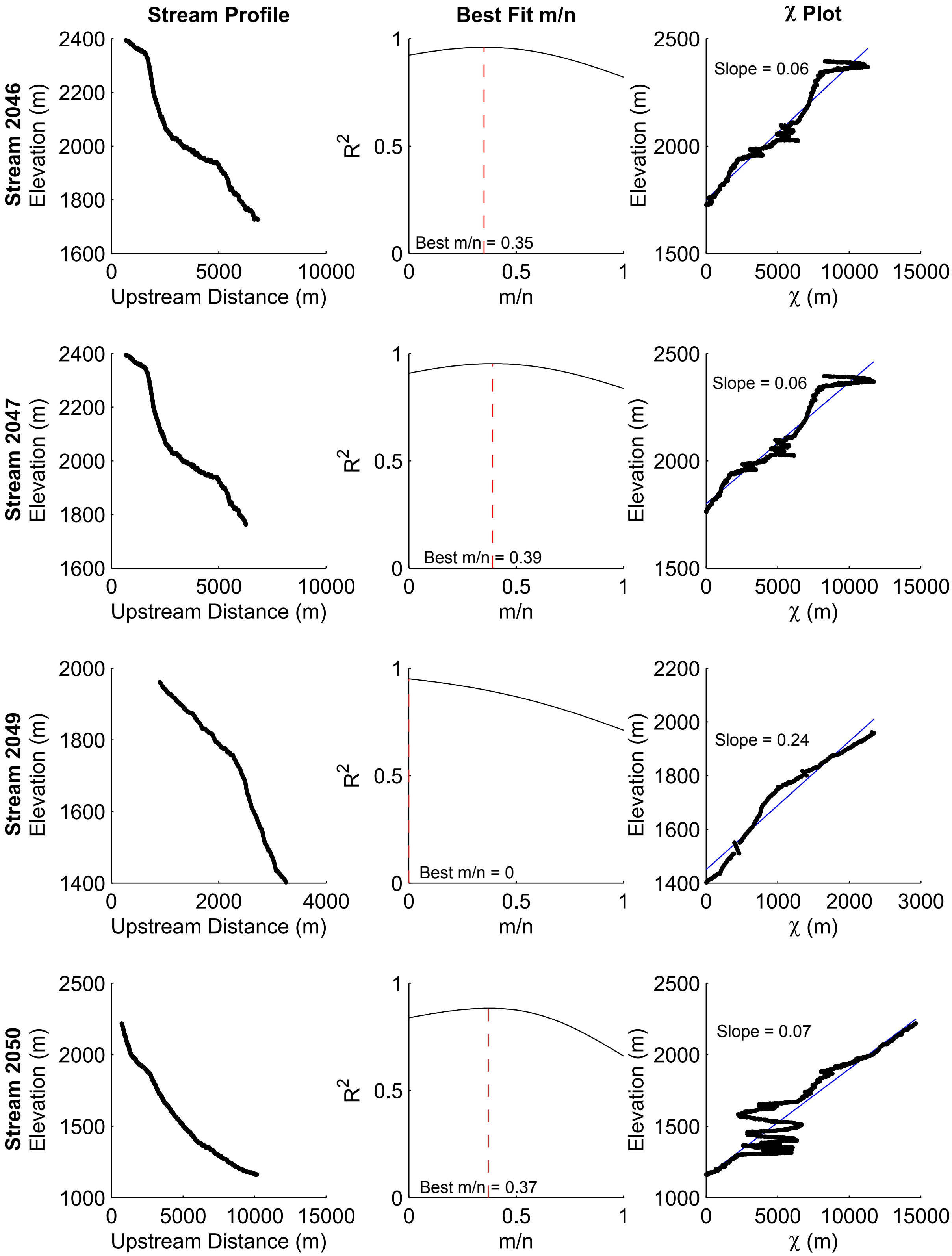
Stream Profile
Best Fit m/n
χ Plot
Stream 2046
Stream 2047
Stream 2049
Stream 2050
Elevation (m)
Upstream Distance (m)
R^2
m/n
χ (m)
Best m/n = 0.35
Best m/n = 0.39
Best m/n = 0
Best m/n = 0.37
Slope = 0.06
Slope = 0.06
Slope = 0.24
Slope = 0.07

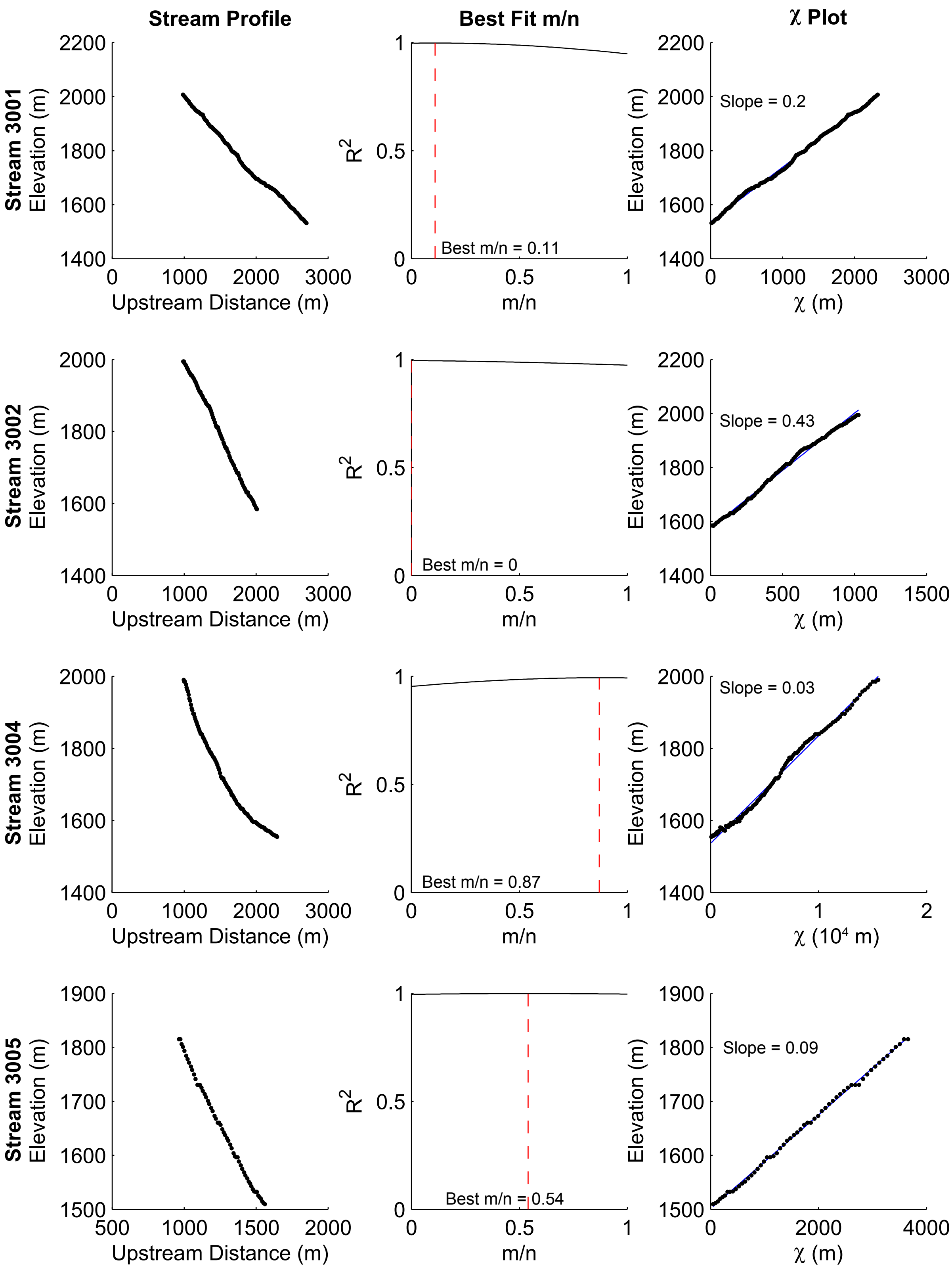
Stream Profile
Best Fit m/n
χ Plot
Stream 3001
Stream 3002
Stream 3004
Stream 3005
Elevation (m)
Upstream Distance (m)
R^2
m/n
χ (m)
χ (10⁴ m)
Best m/n = 0.11
Best m/n = 0
Best m/n = 0.87
Best m/n = 0.54
Slope = 0.2
Slope = 0.43
Slope = 0.03
Slope = 0.09

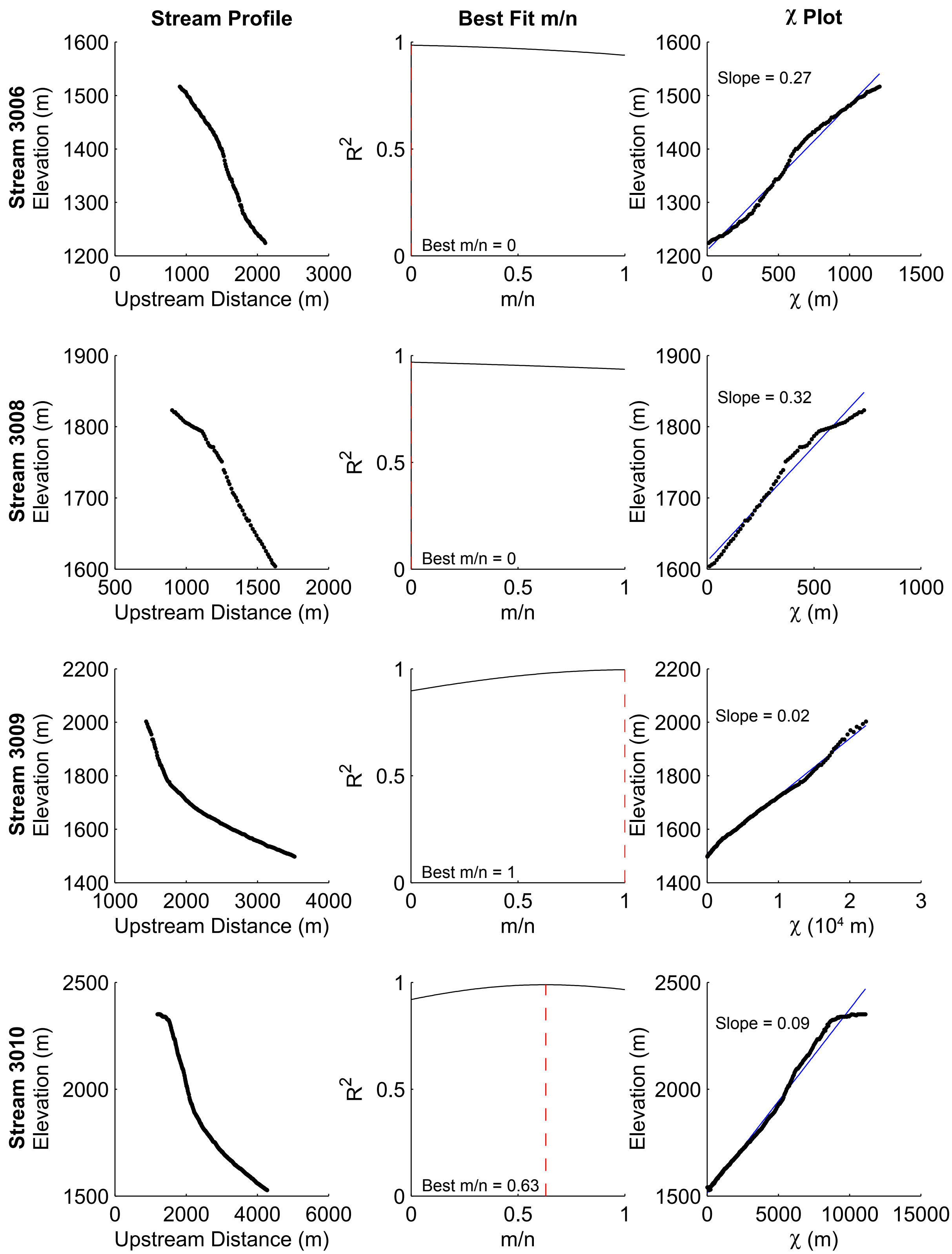
Stream Profile
Best Fit m/n
χ Plot
Stream 3006
Elevation (m)
Upstream Distance (m)
R^2
m/n
Best m/n = 0
Slope = 0.27
χ (m)
Stream 3008
Best m/n = 0
Slope = 0.32
Stream 3009
Best m/n = 1
Slope = 0.02
χ (10^4 m)
Stream 3010
Best m/n = 0.63
Slope = 0.09

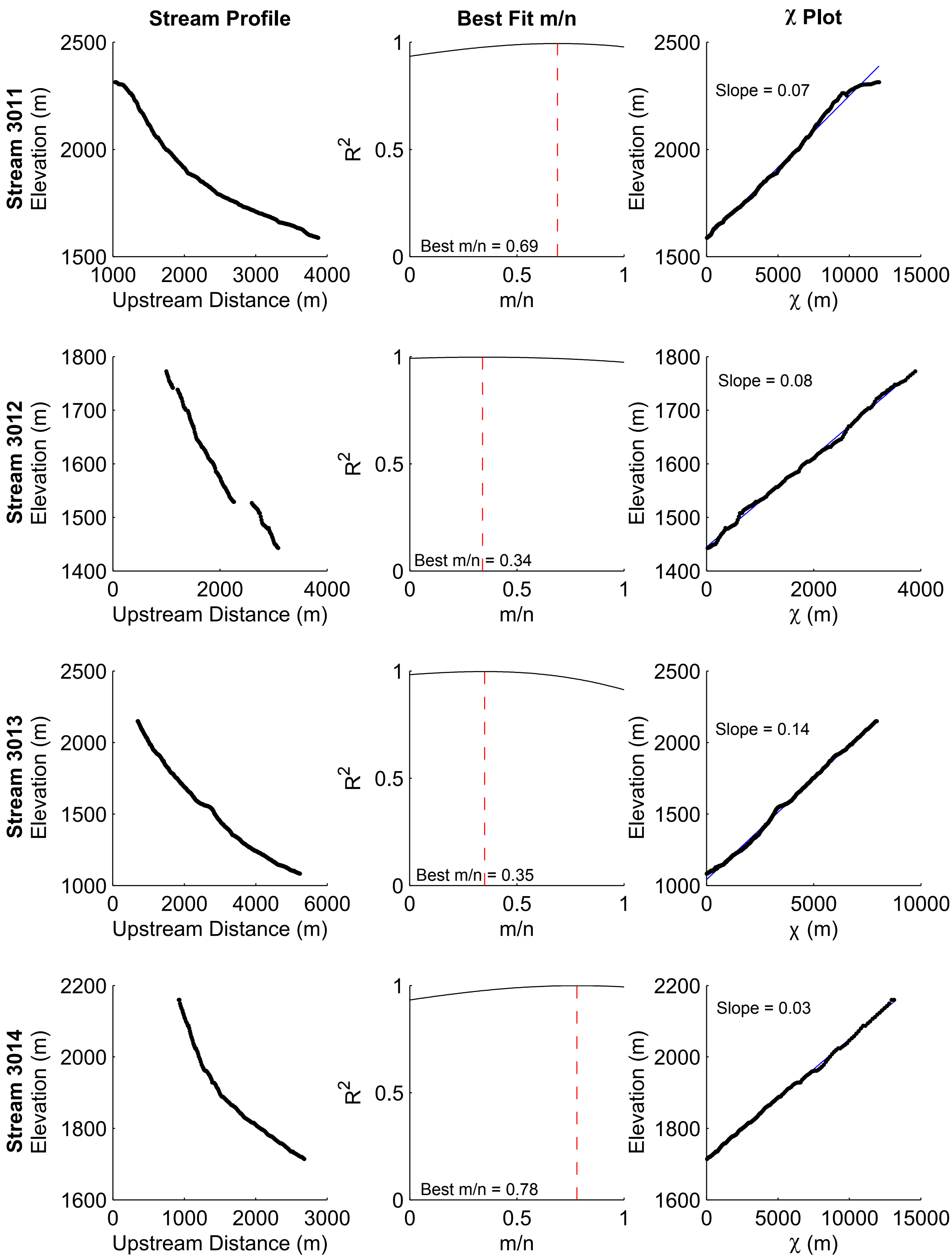
Stream Profile
Best Fit m/n
χ Plot
Stream 3011
Elevation (m)
Upstream Distance (m)
R^2
m/n
Best m/n = 0.69
Slope = 0.07
χ (m)
Stream 3012
Best m/n = 0.34
Slope = 0.08
Stream 3013
Best m/n = 0.35
Slope = 0.14
Stream 3014
Best m/n = 0.78
Slope = 0.03

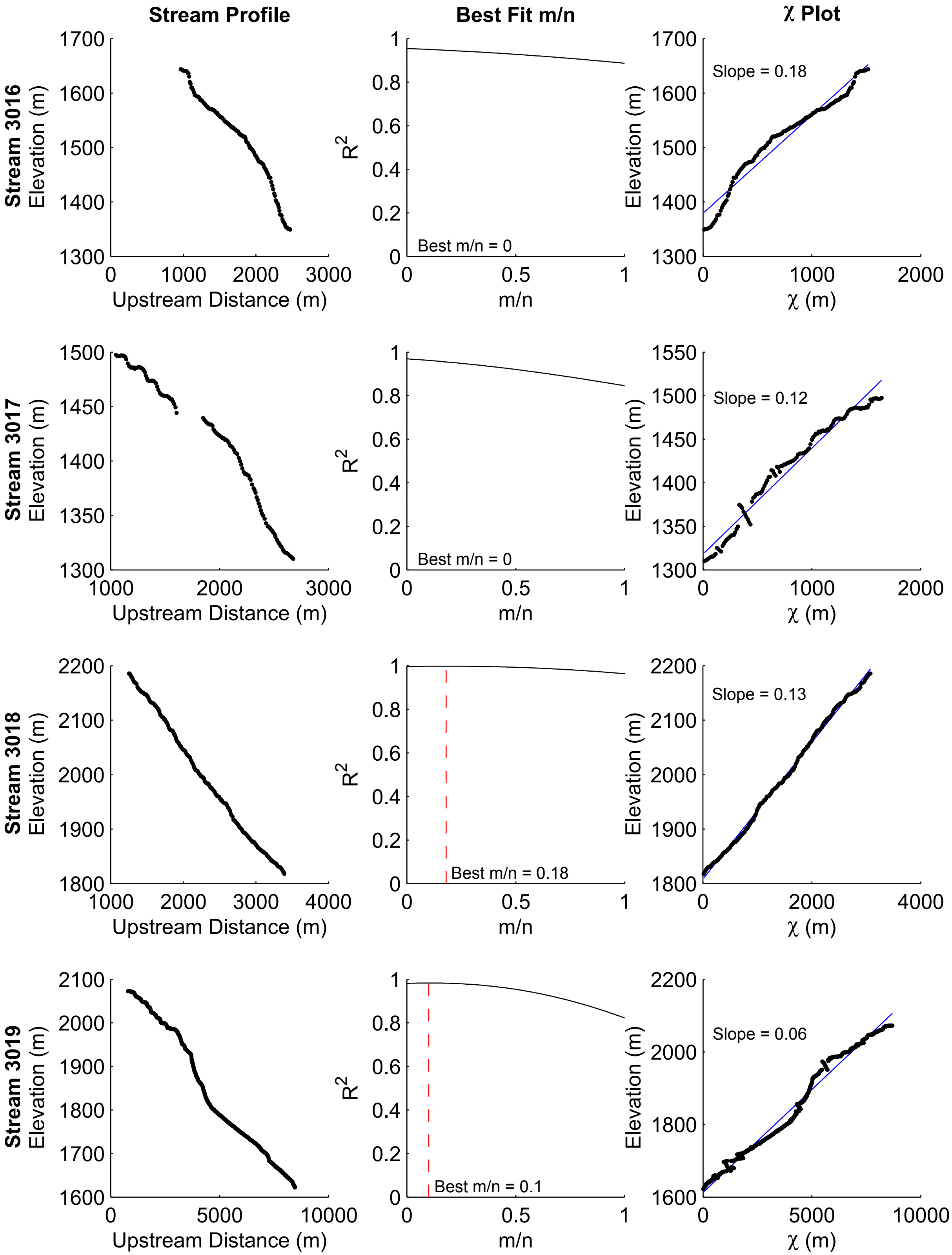
Stream Profile
Best Fit m/n
χ Plot
Stream 3016
Stream 3017
Stream 3018
Stream 3019
Elevation (m)
Upstream Distance (m)
R^2
m/n
χ (m)
Best m/n = 0
Best m/n = 0
Best m/n = 0.18
Best m/n = 0.1
Slope = 0.18
Slope = 0.12
Slope = 0.13
Slope = 0.06

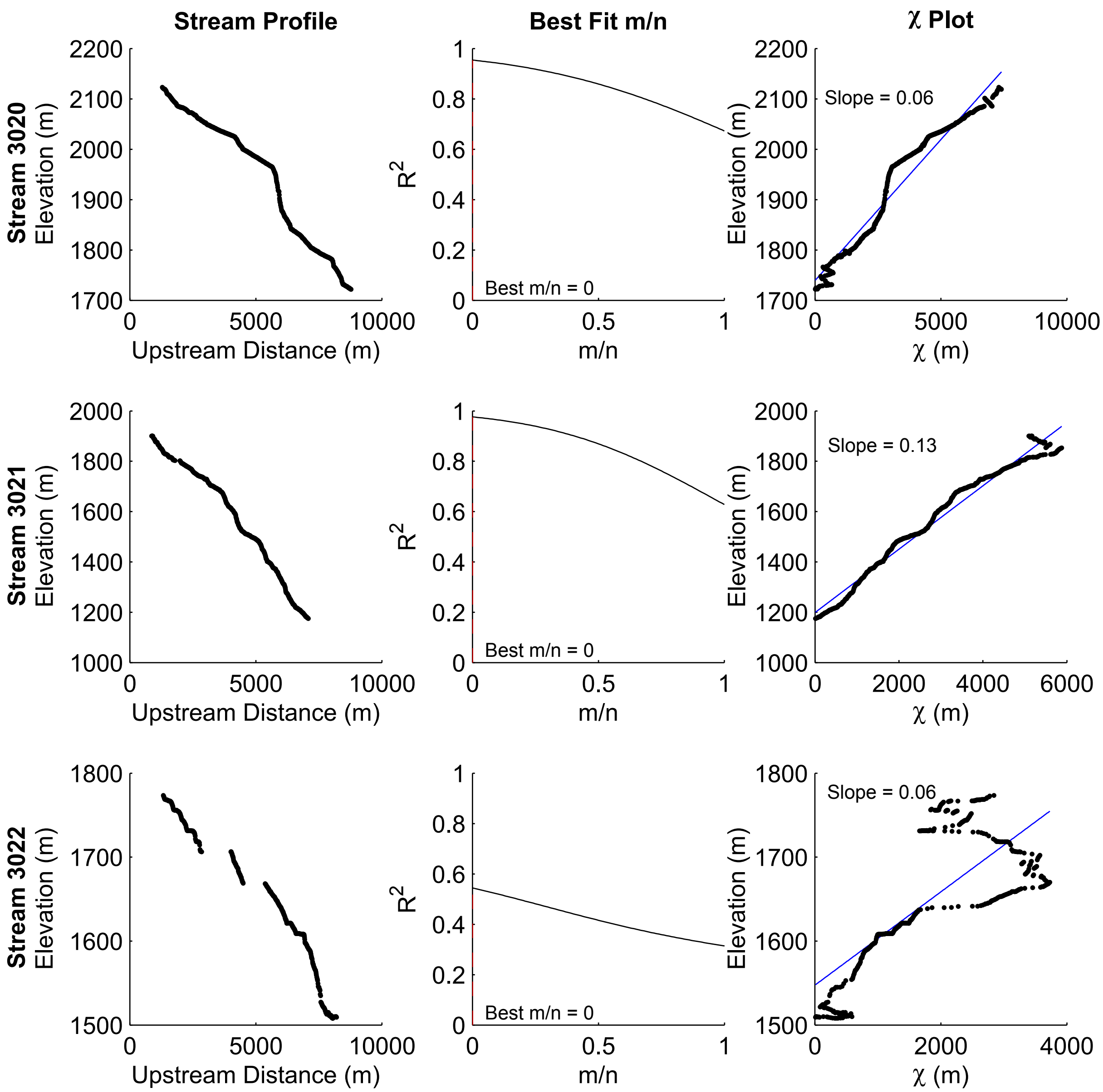
Stream Profile
Best Fit m/n
χ Plot
Stream 3020
Elevation (m)
Upstream Distance (m)
R^2
m/n
Best m/n = 0
Slope = 0.06
χ (m)
Stream 3021
Slope = 0.13
Stream 3022
Slope = 0.06